emerald PUBLISHING

International Journal of Numerical Methods for He
Flui

MODELLING AILERON AND SPOILER DEFLECTIONS WITH THE LINEAR FREQUENCY DOMAIN METHOD (LFD) FOR SUBSONIC FLIGHT CONDITIONS

Journal:	*International Journal of Numerical Methods for Heat and Fluid Flow*
Manuscript ID	HFF-09-2022-0519.R1
Manuscript Type:	Research Article
Keywords:	Linear Frequency Domain Method, Control Surface Surrogate Modelling, Load Alleviation, Load Prediction, LFD, ROM

MODELLING AILERON AND SPOILER DEFLECTIONS WITH THE LINEAR FREQUENCY DOMAIN METHOD (LFD) FOR SUBSONIC FLIGHT CONDITIONS

ABSTRACT

Purpose: The modelling of two surrogate models for predicting the aerodynamic responses of aileron and spoiler control surface's in subsonic flight is presented. The prepared Reduced Order Models prove useful when quick estimations for a large number of variations are required.
Design/Methodology/Approach: The LFD Method was used for the simulation study. Each surrogate contained a database of 100 control surface dynamic responses over a spectrum of 200 harmonics computed with LFD. To interpolate new results, the DLR surrogate modelling toolbox, SMARTy was utilized. The database's samples were prepared in a Halton Sequence, making interpolation reliable. The surrogate's parameter space was the Mach number, Reynold's number, angle of attack, control surface deflection angle, and the control surface chord length.
Findings: The LFD Method proved effective for the mentioned purpose: the surrogates were accurate, up to 15% of relative error, in reproducing dynamic responses of aileron and spoiler deflections at low speed, within the limitations of flow field linearity, as well as surrogate prediction capability. The restrictions of the surrogate, and the reasoning thereof are also presented in detail in the study. Future load alleviation studies are a potential of the findings here.
Originality: LFD is an innovative technique for load prediction and alleviation studies. This paper provides a reference for engineers wishing to use the method for the two mentioned control surfaces, or the like.

Keywords: Linear Frequency Domain, LFD, Surrogate Modelling, ROM, Computational Fluid Dynamics, CFD, Load Alleviation, Load Prediction, Aileron, Spoiler.

NOMENCLATURE

AoA	:	Angle of attack
COR	:	Centre of rotation
c	:	Chord length
c_L	:	Section lift coefficient
c_{L0}	:	Steady state section lift coefficient
f	:	Frequency
im	:	Imaginary part of complex number
k	:	Reduced frequency
l_{ref}	:	Reference length
Ma	:	Mach number
n	:	Harmonic / Mode
$\boldsymbol{R}$	:	Residuals
Re	:	Reynolds number
re	:	Real part of complex number
t	:	Time
$\boldsymbol{u}$	:	State vectors
v_∞	:	Free stream velocity
$\boldsymbol{x}$	:	Grid coordinates
δ	:	Control surface deflection angle
δ_a	:	Aileron deflection angle
δ_s	:	Spoiler deflection angle
$\frac{\partial c_L}{\partial \delta}$	:	Dynamic response magnitude
ρ	:	Density
φ	:	Phase
ω	:	Angular velocity

ω_b : Base angular velocity

1. INTRODUCTION

The aerodynamics of control surface deflections is an important question in many design studies. The dynamic responses of these devices are required for actuator system design, wing design, flight mechanics, and more recently, load alleviation studies. Concerning the case where a large variety of control surface deflections need to be investigated, testing each possibility, dynamically, using the unsteady-RANS approach, can be time consuming and computationally expensive. Furthermore, the validation of such studies in wind-tunnel tests also make the effort tedious. In such cases, where fast results are needed, a surrogate model finds its place. Further contributing to the study would be the linear frequency domain method (LFD), which has proven in the past to efficiently reproduce dynamic responses with reliable accuracy (Seidler *et al.*, 2019), thus having the potential to expedite the preparation of such surrogates as well.

Surrogate models are composed of an accumulation of pre-produced results from experiments or simulation studies. This cloud of data points, known as snapshots, form the basis for interpolating new results within a predefined parameter space. In this study, the DLR surrogate modelling toolbox, SMARTy (Ripepi *et al.*, 2018), was used with its PODI feature: PODI is an extension of the Proper Othogonal Decomposition (POD) method with an interpolation function (Dolci and Arina, 2016). As described by Berkooz *et al.* (1993), the POD method is linear, statistics based and robust for the analysis and synthesis of a wide range of experiments- and simulation-based data. It constructs low-dimensional dynamical models, and with it describes the interactions between coherent structures within the database of information provided. This reduces the problem's complexity and makes finding new results within the database's parameter space computationally inexpensive, while retaining the essential physics of the precomputed results. As the surrogate reduces the high-dimensionality of the problem, a common term for it is a Reduced Order Model (ROM).

In this study, the ROMs were designed for dynamic responses of aileron and spoiler deflections in the low speed flight regime. The results were based on 2D simulations and the cuts were taken from the Airbus XRF1 Concept Aircraft's wing sections. The flight conditions were subsonic. The surrogates served as a database for future load prediction and load alleviation studies, with a potential as a design development and validation tool as well: i.e., the sizing of the control surface actuator systems. This paper details the methodology behind the preparation of these surrogates for the mentioned purposes, with the theory behind the LFD Method being included also. The subsequent validation and/or development studies were not within the purview of this work. Studies by Seidler *et al.* (2019) for flap deflection prediction, described the LFD Method as promising for reducing computation time by up to 6 orders of magnitude compared to standard time-marching techniques.

The same strategy was thus employed here for the current aileron and spoiler problem: the harmonics involved in the deflection of these devices were computed and compiled, in order to be used to produce the dynamic responses of arbitrary deflections as desired. Hence was the problem transitioned from the time domain into the frequency domain with LFD, and the challenges faced with the standard time-marching-techniques were eliminated from the picture. As a result, any aileron or spoiler deflection can be resolved into its various modes via FFT (*Fast Fourier Transform*), and the corresponding dynamic responses of each mode could be superimposed to produce the resultant aerodynamic response of that particular deflection. The results in the frequency domain could then be reconverted back into the time domain via IFFT (*Inverse Fast Fourier Transform*), for ease of viewing. As a final comment, the entire process described in this paragraph is accomplishable approximately within a second with the surrogate.

2. LFD: THEORY AND APPLICATION

The following explanations are based on the DLR TAU User Guide's description of the LFD Method. At the end of this section the application of the method in this study will be provided.

$$\frac{d\boldsymbol{u}}{dt} + \boldsymbol{R}(\boldsymbol{u}, \boldsymbol{x}, \dot{\boldsymbol{x}}) = 0 \tag{1}$$

Equation (1) is the governing equation of an unsteady flow field. It states that the flow field's state vectors, $\boldsymbol{u}$, i.e. the velocity, pressure, temperature and density, are conserved. In a discretized system, an added residual component of the state vectors, $\boldsymbol{R}(\boldsymbol{u}, \boldsymbol{x}, \dot{\boldsymbol{x}})$, become present to uphold this conservation criterion; $\boldsymbol{x}$ is the grid position vector while $\dot{\boldsymbol{x}}$ is the grid velocity vector.

A Reynolds decomposition of the fluctuating state vectors and oscillating grid motion is performed to model the flow field as a steady mean flow with a perturbation component:

$$\boldsymbol{u}(t) = \bar{\boldsymbol{u}} + \tilde{\boldsymbol{u}}(t) \quad \|\tilde{\boldsymbol{u}}\| \ll \|\bar{\boldsymbol{u}}\| \tag{2}$$

$$\boldsymbol{x}(t) = \bar{\boldsymbol{x}} + \tilde{\boldsymbol{x}}(t) \quad \|\tilde{\boldsymbol{x}}\| \ll \|\bar{\boldsymbol{x}}\| \tag{3}$$

$$\dot{\boldsymbol{x}}(t) = \dot{\tilde{\boldsymbol{x}}}(t) \tag{4}$$

A prerequisite for further analysis is that the perturbation components, $\tilde{\boldsymbol{u}}$ and, $\tilde{\boldsymbol{x}}$ are kept small. This limits the consideration to linear flow fields, and enables the further modelling of the perturbation components as periodic oscillations. These can then be described as Fourier series (Equations (5) and (6)), thus switching the problem from the time domain into the frequency domain. This means that only the modes of oscillation present in the flow field need to be solved for, instead of solving the governing equations directly.

$$\boldsymbol{u}(t) = \bar{\boldsymbol{u}} + \sum_n \hat{\boldsymbol{u}}_n e^{in\omega_b t} \tag{5}$$

$$\boldsymbol{x}(t) = \bar{\boldsymbol{x}} + \sum_n \hat{\boldsymbol{x}}_n e^{in\omega_b t} \tag{6}$$

Applying equation (5) and (6) to equation (1), the following results:

$$\left\{in\omega_b \boldsymbol{I} + \frac{\partial \boldsymbol{R}}{\partial \boldsymbol{u}}\right\}\hat{\boldsymbol{u}}_n = -\frac{\partial \boldsymbol{R}}{\partial \boldsymbol{x}}\hat{\boldsymbol{x}}_n - in\omega_b \frac{\partial \boldsymbol{R}}{\partial \dot{\boldsymbol{x}}}\hat{\boldsymbol{x}}_n \tag{7}$$

The flow field is now described in terms of the modes of oscillations present in the flow. The left-hand side (LHS) of equation (7) describes the relation between the Fourier coefficient of the state vectors, $\hat{\boldsymbol{u}}_n$, with the flux Jacobian, $\partial \boldsymbol{R}/\partial \boldsymbol{u}$, and the mode of oscillation in the flow, ω_b; the right-hand side (RHS), in turn, connects the grid coordinate coefficient, $\hat{\boldsymbol{x}}_n$, with the Jacobians of the residuals with respect to: 1) the grid coordinates, $\partial \boldsymbol{R}/\partial \boldsymbol{x}$ and 2) the grid coordinate velocity, $\partial \boldsymbol{R}/\partial \dot{\boldsymbol{x}}$; the mode of oscillation of the flow field, ω_b also being a factor in consideration. Essentially, equation (7) simply states, that the state-vectors of the flow field respond linearly to the motion in the grid space, depending on the mode of oscillation present in the flow.

Equation (7) is solved numerically, and is hence treated in two parts: the RHS first, followed by the LHS. The RHS is defined based on the component's oscillation, which, in equation (7), is described in terms of the Fourier coefficients of the grid coordinates and its corresponding grid coordinate and coordinate velocity Jacobians. With the RHS well defined, the LHS can be iteratively solved for the state vectors, $\hat{\boldsymbol{u}}_n$. Considering a small angled oscillation, the first harmonic would be dominant; this further simplifies solving equation (7). Readers interested in a rigorous and thorough explanation of equation (7) are directed to the paper by Widhalm and Thormann (2017).

If 1 harmonic can be solved in this manner, a series of harmonics relevant to the control surface deflection can be solved as a series of computations, producing a spectrum of dynamic responses for each flight condition investigated. Each spectrum is then, a snapshot for the ROM.

3. THE SURROGATE MODEL'S PROCESS CHAIN

The ROM's process chain is displayed in Figure 1 below:

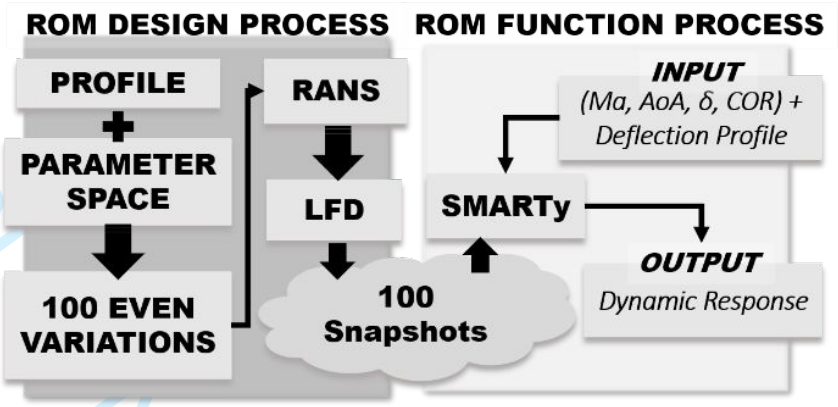

Figure 1. Surrogate design and function process chain.

The first part of Figure 1 depicts the design process flow of the surrogate model using LFD. The database of the surrogate comprises of data points known as snapshots. A snapshot contains the dynamic responses of the model's control surface deflection over a predefined frequency range. Each snapshot however is simulated for a certain flight condition with the aerofoil configured to that particular flight condition: hence it is a geometric variation of the base profile. The mentioned variations in geometric and aerodynamic conditions are prepared such that the surrogate contains an even distribution of data points. This is accomplished by generating a Halton Sequence (Berblinger and Schlier, 1991; Berkooz *et al.*, 1993) of parameter combinations within the surrogate's parameter space (See Parameter Space Definition Section for details of the ROM's parameter space). 100 such variations were created for the simulation study and a stable RANS solution for each variation was prepared. Subsequently, the dynamic responses for a range of 200 frequencies were computed with LFD based upon each of the aforementioned RANS solutions. This database, when compiled, formed the surrogate model which could be used with the DLR Surrogate Modelling Toolbox, SMARTy to interpolate new dynamic response information for a given parameter combination. The interpolation would yield reliable results so long as the desired parameter combination remains within the defined parameter space of the ROM.

4. PARAMETER SPACE DEFINITION

The parameter space of the surrogate model was so defined to encompass all possible conditions relevant for the investigation, as well as to describe the aerodynamic problem investigated as simply as possible. Hence, the aerodynamic flow field was specified based on the Mach number, *Ma*, Reynolds number, *Re*, and the angle of attack, *AoA*, while the geometric parameters of the problem were defined as the control surface deflection angle, δ, and the control surface chord length, varied by shifting its centre of rotation, *COR*, along the profile's chord. The control surface chord length was thereby parametrized in the study as the ratio of the control surface's chord to the profile's chord. Table I and II below details the parameter space defined for the surrogates in this study:

Table I. Aileron Surrogate's Parameter Space

Mach number, *Ma*	0.12 - 0.35
Reynolds number, *Re*	1.2e7- 3e7
Angle of attack, *AoA*	2° - 8°
Aileron deflection angle, δ_a	0 - +10°
Ratio of aileron chord to profile chord	0.1 – 0.3

Table II. Spoiler Surrogate's Parameter Space

Mach number, *Ma*	0.12 - 0.35
Reynolds number, *Re*	1.2e7 - 3e7
Angle of attack, *AoA*	2° - 8°
Spoiler deflection angle, δ_s	0 - +5°
Ratio of spoiler chord to profile chord	0.1 - 0.15

5. BASE PROFILE

The profiles chosen for the purpose of this study were taken from the Airbus XRF1 Concept Aircraft. The study was conducted in 2D, since the linear frequency domain solver showed good promise of two-dimensional results in previous studies (Seidler *et al.*, 2019). Two profiles were extracted, the first from the outboard spoiler/flap section of the wing, while the second from the outboard aileron section. Figure 2 below describes the control surface layout and positions for the profile extractions.

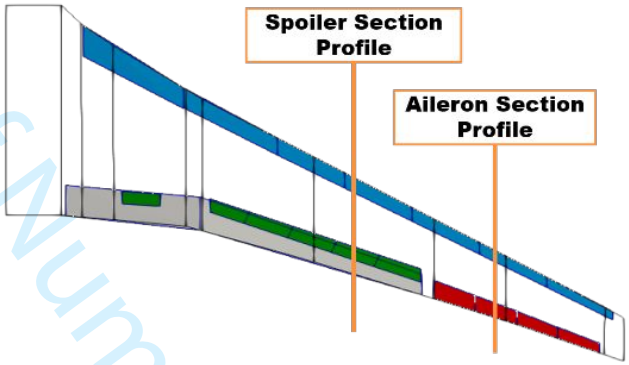

Figure 2. Control surface layout of the XRF1 Concept Aircraft.

These positions were chosen where 3D flow effects were expected to be minimum. This meant that the 2D studies would be relatively comparable to the 3D case.

Transition areas between control surface zones were therefore avoided and profiles were chosen from as far a distance as possible from the fuselage-wing intersection area. The mid-section of the aileron and spoiler was used for the profile cut-outs in order to minimize flow effects at the gaps between each control surface. The base profiles were extracted in the take-off configuration.

6. MODELLING THE CHOSEN PROFILES

The profiles chosen were subsequently scaled according to the wing's leading-edge sweep angle to model the flow simulation study in 2D. As a feature for control surface sizing, the centre of rotation of the control surface, *COR*, measured from the profile's leading edge, was varied between 70% - 90% of the profile's chord length. The control surface chord length was thereby the first geometric parameter of each surrogate model. The second geometric variation of the model was the deflection angle of the control surface, δ. To model this, the aileron and spoiler of the base profiles were deformed for each deflection angle prepared in the parameter space. This was accomplished via a python script by extracting the geometry points of the model and performing a simple coordinate transformation of these points about the given centre of rotation with the deflection angle being the required input. A small section of the profile about the rotation point of the deflected section was cut out and a spline was generated to connect the transformed section to the fixed section of the geometry, thus ensuring a smooth profile for computation purposes.

An example of the model variation for the aileron is featured in Figure 3, while Figure 4 depicts the model variation of the spoiler.

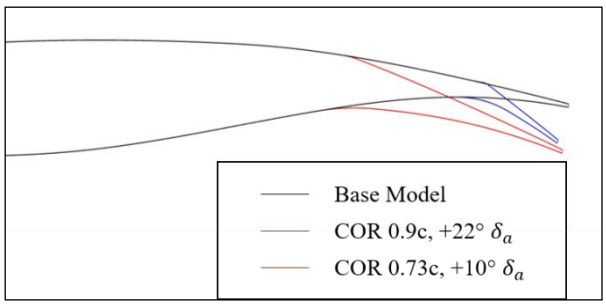

Figure 3. Modelling of the aileron deflection.

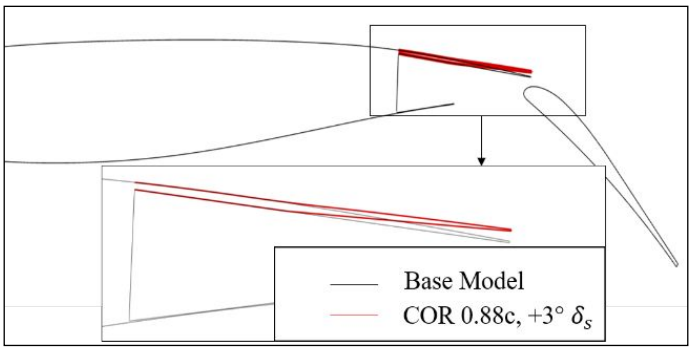

Figure 4. Modelling of the spoiler deflection.

7. MODEL GRIDS

The grid generation was carried out only for the base profiles cut out from the wing sections of the concept aircraft. The grids contained around 100,000 points each and were deformed with the Radial Basis Method according to the 100 geometry variations prepared in the previous section. This ensured that the number of grid points remained constant for all the simulated samples. Examples of the deformed aileron section and spoiler section are shown in Figure 5 and 6 respectively:

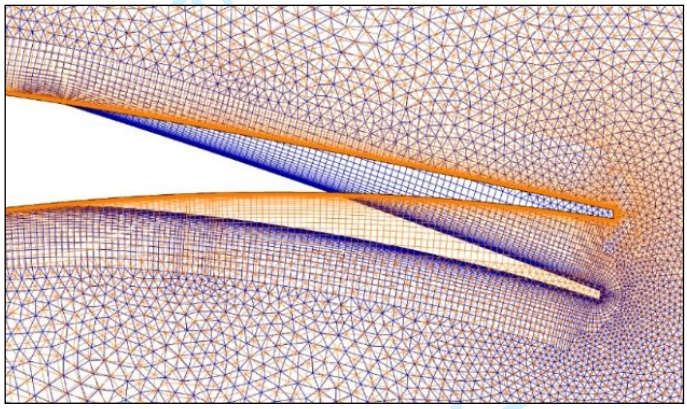

Figure 5. Mesh deformation of the aileron section (*COR* at 76% chord length; deflection angle: 8.52°).

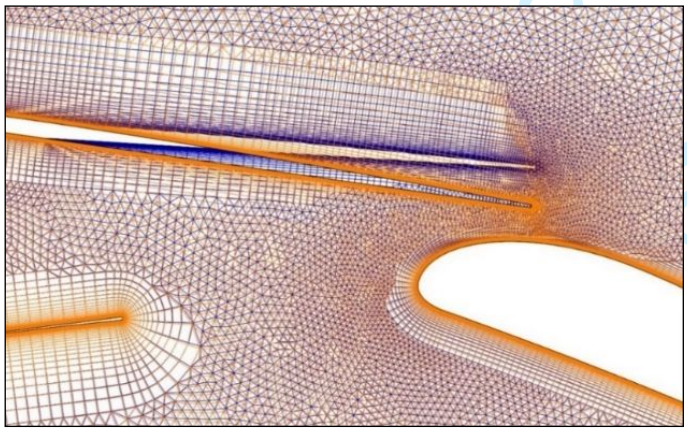

Figure 6. Mesh deformation of the spoiler section (*COR* at 86% chord length; deflection angle: 4.51°).

8. MODELLING THE RIGHT-HAND SIDE (RHS) OF EQUATION (7) FOR THE LFD FLOW SOLVER

As mentioned in Section 2, if the Fourier coefficient of the grid nodes, $\hat{\boldsymbol{x}}_n$, is known, the coefficient of the state vectors, $\hat{\boldsymbol{u}}_n$, can be iteratively derived by the LFD-Solver. Hence, it is important to first compute the RHS of the equation by defining $\hat{\boldsymbol{x}}_n$, the grid motion. This was carried out with reference to a small angled deflection of the relevant control surface. The chosen angle of deflection in this study was ±1 degree. The grid in the vicinity of the deflected control surface was subsequently deformed with the Radial Basis Function. This also ensured that the number of grid nodes were kept constant, an important criterion in solving the RHS of equation (7). Subsequently, the grid node Jacobian, $\partial \boldsymbol{R}/\partial \boldsymbol{x}$, and the grid node velocity Jacobian, $\partial \boldsymbol{R}/\partial \dot{\boldsymbol{x}}$, were provided to the LFD Solver. An example of the above-mentioned aileron deflection is depicted in Figure 7 below:

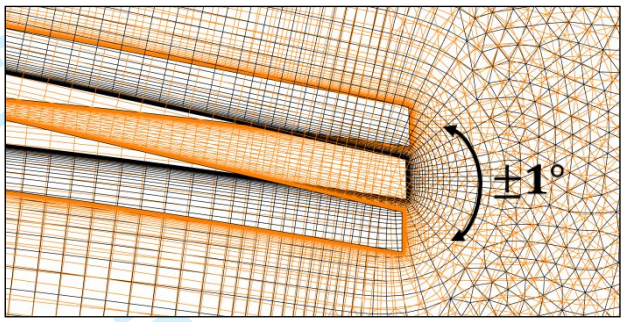

Figure 7. Modelling of a ±1-degree aileron deflection in DLR-TAU Code with the Radial Basis Function Method.

9. RANS SOLUTIONS

As emphasized in equation (2), a steady mean state solution is a prerequisite for usage of the LFD Method. A stable RANS solution was therefore prepared for each model variation in their respective flight conditions. All computations were done using a single node comprising of a dual socket AMD EPYC 7601 microprocessor in the DLR CARA Cluster. The following are the RANS solutions produced in this study: the first in Figure 8 is for the 100 aileron control surface variations while the second in Figure 9 is for the spoiler, prepared in a similar way. The one equation Spalart-Allmaras turbulence model (Spalart and Allmaras, 1992) was used for the mentioned RANS simulations.

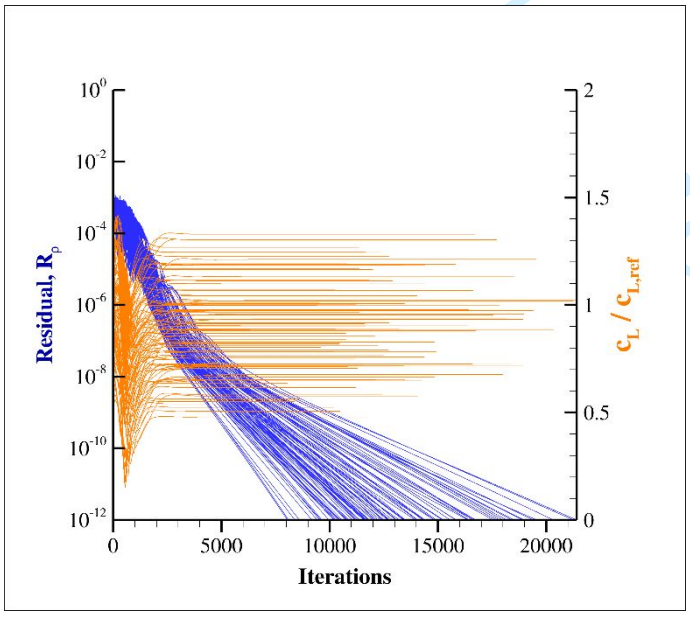

Figure 8. RANS solution for Halton sequence of 100 parameter combinations (Aileron section profile in take-off configuration with 15° slat and 10° flap deflection at mean sea level (MSL) conditions); Reference flight condition: Ma = 0.25; Re = 2.2e7; AoA = 7.02°; δ_a = 3.28°; COR = 0.9.

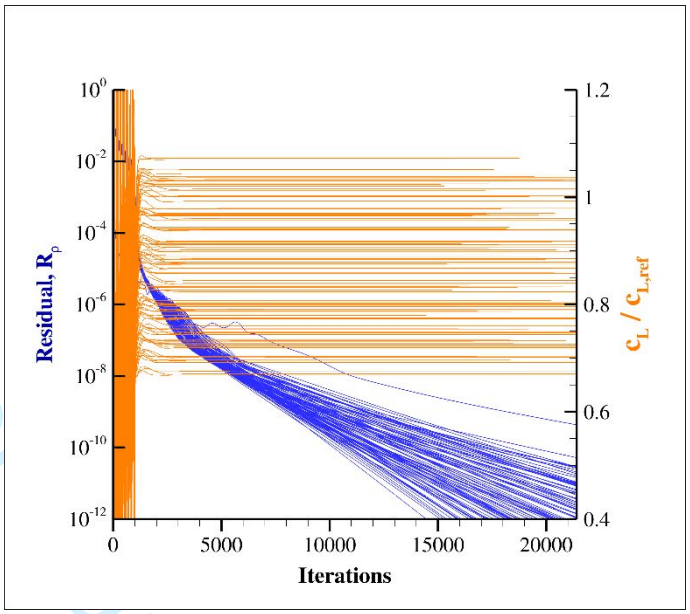

Figure 9. RANS solution for Halton sequence of 100 parameter combination (Spoiler section profile in take-off configuration with 15° slat and 10° flap deflection at mean sea level (MSL) condition); Reference flight condition: Ma = 0.25; Re = 3.2e7; AoA = 7.02°; δ_s = 3.36°; COR = 0.9.

As can be seen from both figures above, the steady-state simulations with the SA-Turbulence Modell produced a good convergence of the lift coefficient, c_L, with residuals of density converged by 12 orders of magnitude. The degree of residual drop was in accordance with the recommendations in (Seidler *et al.*, 2019); whereby a convergence of at least 10 orders of magnitude is required for adequate computational convergence with the linear frequency domain method. The above 200 Halton Sequence samples (100 samples for each profile) were therefore deemed appropriate as a basis for the subsequent computations with LFD.

10. LFD SOLUTIONS

With the RANS solutions prepared and the RHS of equation (7) solved, the linear frequency domain solver could then compute the desired dynamic responses for a set of predefined frequencies for each RANS solution: this defines a single snapshot.

The simple trapezoidal flap deflection profile in (Seidler *et al.*, 2019) was adopted as a generic case for the analysis in this study. This was seen as reasonable since the deflections of an aileron or spoiler can be modelled in 2D as a simple deflection about a hinge in the profile itself without any fowler extension. Hence, the considerations for the frequency modes generated by a simple control surface component oscillating about a hinge in a flow were adopted and used in this study as well.

Another point of interest was the definition of the oscillating frequencies in the flow field: since the standard measure for the unsteadiness of a flow field is the reduced frequency, k, this was appropriate for use in this study. For clarity, the definition of the reduced frequency, k, is given below:

$$k = \frac{\omega * l_{ref}}{v_\infty} \tag{8}$$

As detailed in (Seidler *et al.*, 2019), the dominant modes for a standard flap deflection problem is known to occur in the lower reduced frequency range of $k \leq 0.2$. However, even taking a maximum 100 °/s flap deflection into consideration, which translates to 0.28 Hz, a conservative range of frequencies extending beyond this limit was included in this study. This was done, since in the case of an arbitrary deflection of a control surface, while a multitude of modes constitute the description of that particular deflection, and while the most dominant frequencies would describe its motion well enough, a higher resolution of modes would definitely improve the prediction of the deflection profile; especially when considering quick changes in control surface movement. Hence, a band of frequencies up to k = 3 was simulated in this study. This translates to a control surface oscillation of up to 40 Hz for the low speed condition investigated here.

The LFD solver computes the relevant coefficients of state vectors, $\hat{\boldsymbol{u}}_n$, and with it derives the dynamic responses of each frequency of oscillation, in a complex valued form, giving the real and imaginary components

of the dynamic response. In this case study, the dynamic response of the lift coefficient is emphasized. The magnitude and phase of the aerodynamic response computed by the LFD solver is defined below:

$$\frac{\partial c_L}{\partial \delta}(\omega) = \sqrt{\left(\frac{\partial \hat{c}_L}{\partial \delta}\right)_{re}^{2} + \left(\frac{\partial \hat{c}_L}{\partial \delta}\right)_{im}^{2}} \tag{9}$$

$$\varphi(\omega) = \tan^{-1}\left(\frac{\left(\frac{\partial \hat{c}_L}{\partial \delta}\right)_{im}}{\left(\frac{\partial \hat{c}_L}{\partial \delta}\right)_{re}}\right) \tag{10}$$

The spectrum of dynamic responses for the defined frequency range is shown for the aileron deflections in Figure 10 and for the spoiler deflections in Figure 11. Although the surrogates were prepared with reference to the reduced frequency, k, for ease of displaying all 100 snapshots in a single diagram, the frequency, f, ranging from 0 - 40 Hz instead of k was used as the horizontal axis in both Figure 10 and 11. The computation time per frequency was around 13.5 sec, with 200 frequencies completed in about 45 minutes to an hour with the same computational resource used for the RANS simulations.

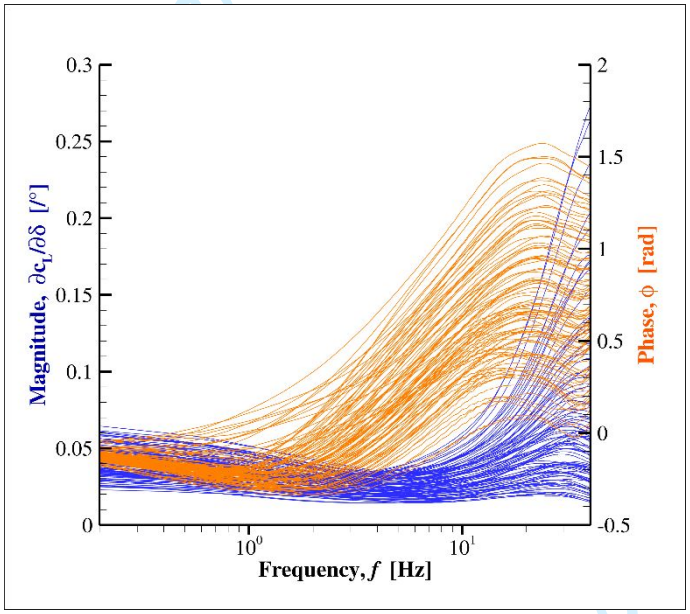

Figure 10. Magnitude and phase diagram of the dynamic responses for an aileron deflection over a frequency range of 0 - 40 Hz.

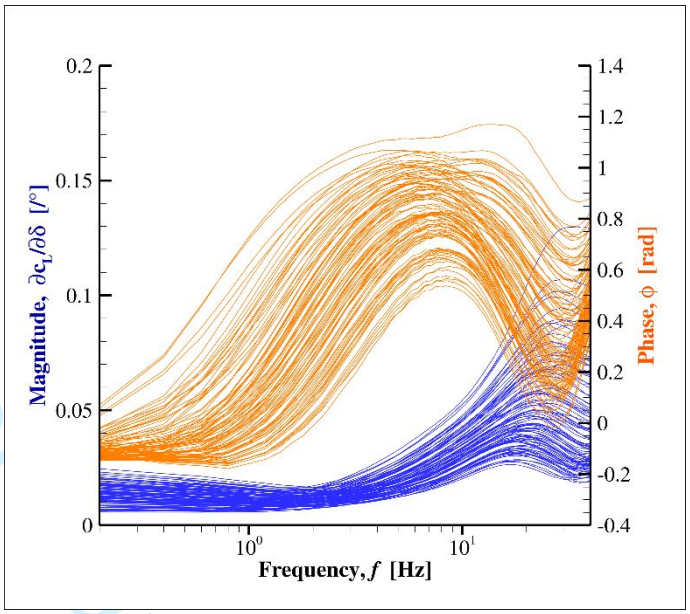

Figure 11. Magnitude and phase diagram of the dynamic responses for a spoiler deflection over a frequency range of 0 - 40 Hz.

As can be seen from both figures, the magnitude drops asymptotically to 0 with reducing frequencies. This is naturally the case, since a stationary flow ($f = 0$ Hz) cannot generate a dynamic response.

From Figure 10 for the aileron deflection case, a successive change in the dynamic response can be observed throughout the frequency spectrum. The dynamic response magnitude initially drops slightly by about 0.015 [/°] from 0 to 6 Hz, before rising towards their respective maximum magnitudes at around 30 Hz. The dynamic response magnitude for all cases begin to slowly decrease again with increasing frequency. The most drastic increment in magnitude is recorded to be 0.2 [/°] for the flow condition listed here: $Ma = 0.12$; $Re = 1.05e7$; $\delta_a = 9.1°$; $AoA = 4.38°$.

The phase profile is seen to be relatively low under 2 Hz, varying between -0.3 to +0.3 rad. The phase of the dynamic responses of the aileron deflections however begin to rise from 3 Hz onwards up to a maximum φ value of 1.6 rad at 20 Hz. Beyond this frequency the phase of all cases begins to fall by around 0.2 rad.

The spoiler response behavior in Figure 11 also portrays a slight initial drop of around 0.0025 [/°] from 0 - 2 Hz, before increasing by about 0.078 [/°] towards 25 Hz. Following this, the magnitude response of all cases falls by about 0.01 [/°] towards 40 Hz.

In regards to the phase, the same asymptotic behavior is observed when approaching a stationary flow condition. Generally, an increasing phase for all cases up to an average value of 0.85 rad at 7 Hz is observable. The phase then decreases gradually towards 25 Hz by an average value of around 0.4 rad, before finally rising again as the frequency increases up to 40 Hz.

Various different flow effects in the oscillating flow field could influence the dynamic response behavior as portrayed in Figure 10 and 11. What is however important in this study is that the dynamic response of each snapshot is comparable to one another in Figure 10 and 11 above. This implies that throughout the investigated parameter space of the study of each ROM, the aerodynamic flow conditions do not vary drastically from one another: a database of similar samples would lead to an improved accuracy in interpolation. The gradual shift of phase and wave like change in the dynamic response behavior also implies that the LFD solutions for each frequency are well converged and all cases remain as asserted by the previous RANS solutions within the bounds of linearity: a non-linear flow field or non-converged LFD solution would generate noticeable variations between each dynamic response over the frequency range.

11. THE SURROGATE QUALITY CHECK: THE LEAVE-ONE-OUT TEST

The quality of the ROMs produced were verified via a standard Leave-One-Out Test procedure. The test required each surrogate to reproduce a snapshot via its interpolation algorithm with a low relative error, should that snapshot be removed from the surrogate. If accomplished, it would imply two things, namely, that the ROM can reproduce new results reflecting the physics of the high-fidelity solutions, and, that the removal of one snapshot doesn't impair the surrogate's ability to interpolate correct results. In other words, the snapshot density within the surrogate

is sufficient for reliable interpolations to take place. Furthermore, the removed snapshot, when added back in, can only promote better accuracy for the surrogate to interpolate new results within the database. An example of such a quality check is shown in Figure 12 to 15, with relative errors being safely below a tolerable 15%. Since the dynamic response computed is based upon the static lift coefficients computed via the aforementioned RANS simulations, both are an integral part of each surrogate model.

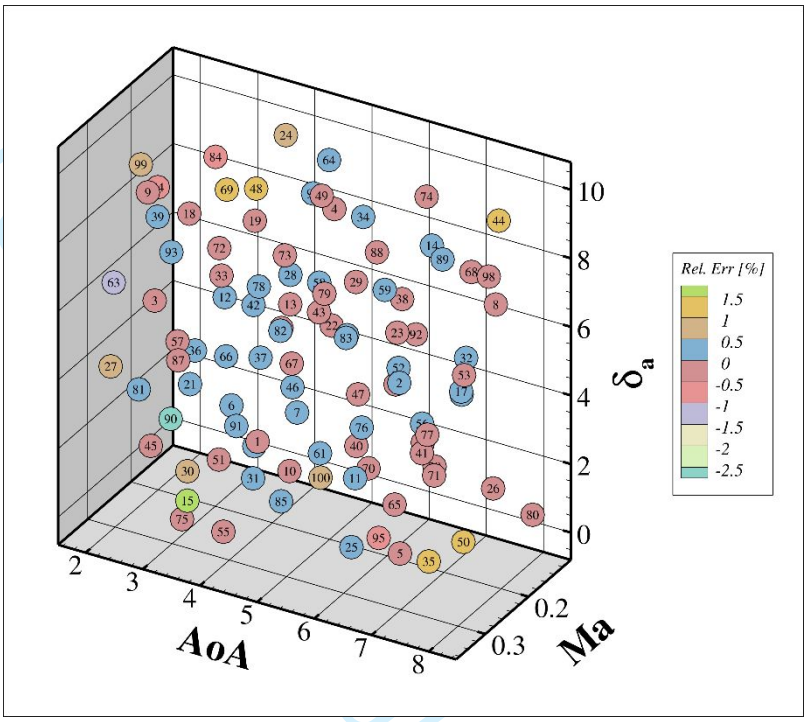

Figure 12. 3D plot of the aileron surrogate's Leave-One-Out Test for the interpolation of the static section lift coefficient, c_L; data points numbered according to Halton sequence.

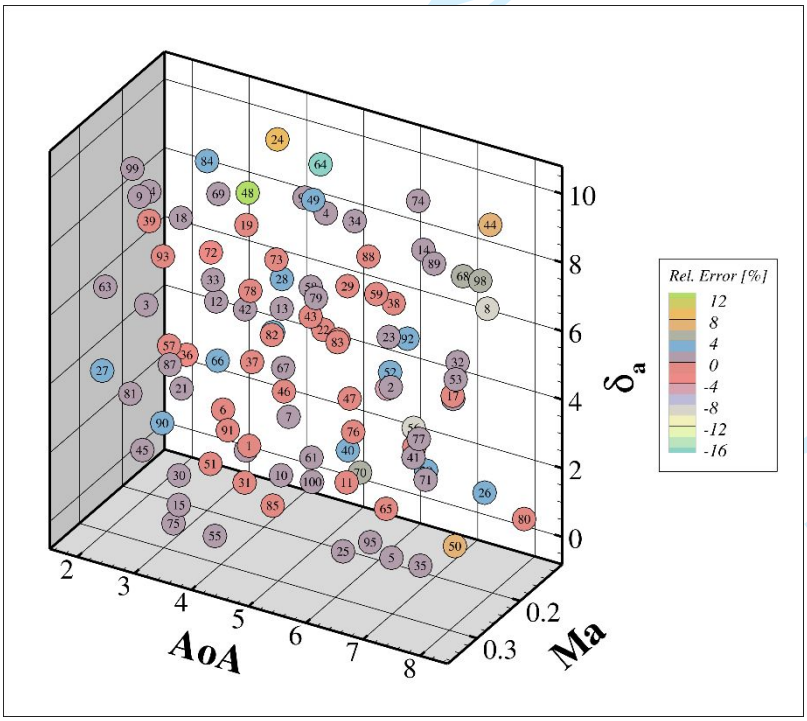

Figure 13. 3D plot of the aileron surrogate's Leave-One-Out Test for the interpolation of the dynamic response; data points numbered according to Halton sequence.

In the case of the aileron surrogate model, the majority of cases show a relative error of less than 0.8% for the interpolation of the static lift coefficient. As for the interpolation of the dynamic response itself a relative

error of 8% is observed for most cases. A few outliers with a relative error of 2.4% is observed for the static lift coefficient interpolation while an outlier of 15% is observable for the interpolation of the dynamic response of the aileron deflection.

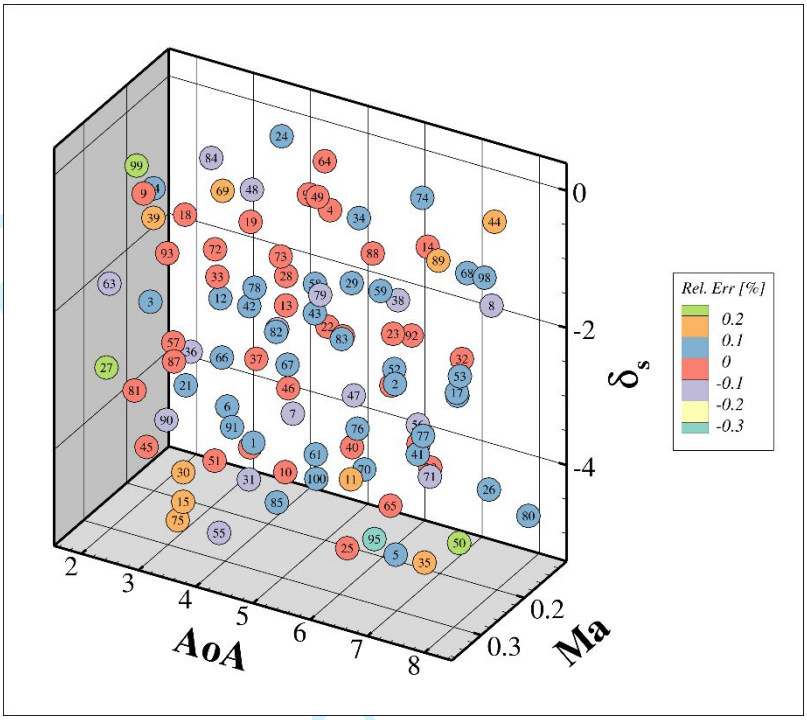

Figure 14. 3D plot of the spoiler surrogate's Leave-One-Out Test for the interpolation of the static section lift coefficient, c_L; data points numbered according to Halton sequence.

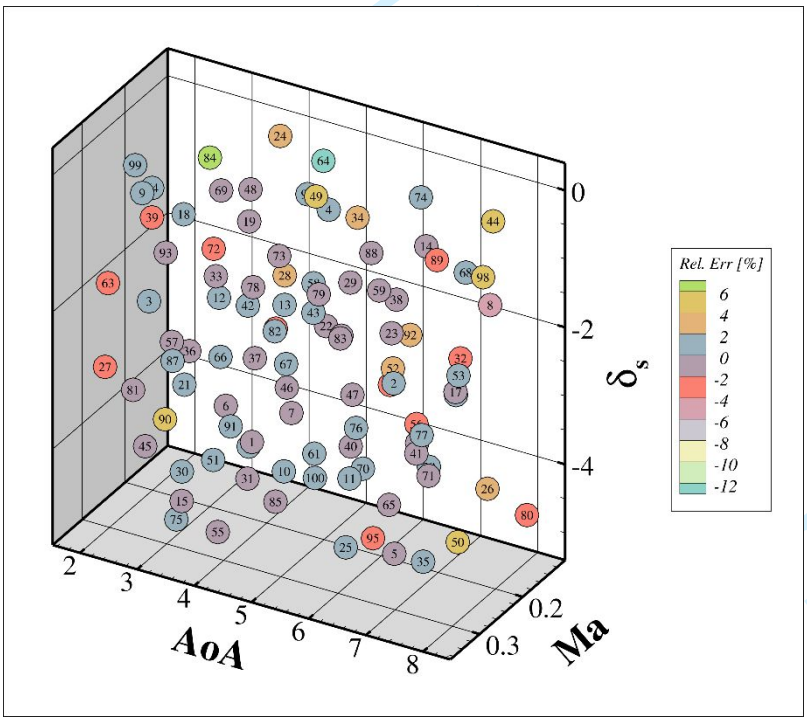

Figure 15. 3D plot of the spoiler surrogate's Leave-One-Out Test for the interpolation of the dynamic response; data points numbered according to Halton sequence.

As for the spoiler deflection case, the interpolation of the static lift coefficient happens generally with a relative error of under 0.3%. The interpolation algorithm of the SMARTy toolbox produced a relative error under 6% in the case of the dynamic response of a spoiler deflection. The only outlier for this surrogate model was a sample which produced a relative error of 13.5%.

Overall both models still showed a good interpolation capability which make them reliable for use. An important factor to note is that the outliers in both surrogates tend to involve samples which lie at the edge of the surrogate's parameter space. This is understandable, as the interpolation algorithm of the SMARTy toolbox requires sufficient snapshots in the vicinity of the desired interpolation point to make a relatively accurate interpolation. At the edge of the parameter space, where such an availability of snapshots is scarce, a larger relative error is expected, since potentially different flow behaviour captured in the rest of the parameter space would weigh in to the quality of the interpolation. It is hence a recommended practice to always ensure that the parameter space for which a surrogate is designed lies as close as possible to the centre of the surrogate's parameter space. A ROM must therefore at best be modelled for a much larger parameter space than its intended use. A second risk involves straying too far off at the edge of the parameter space, where different flow effects begin to occur. As a result, the interpolations within the surrogate will be influenced by these effects, causing unnecessary errors, reducing the surrogate's reliability. Therefore, while the parameter space of the surrogate should be made as large as possible, it is also prudent to ensure that the flow field within the investigated parameter space remain similar in behaviour to guarantee reliable interpolations by the surrogate model.

12. APPLICATION EXAMPLES

Eight application examples are provided here to demonstrate each ROM's prediction capability in comparison to URANS simulations.

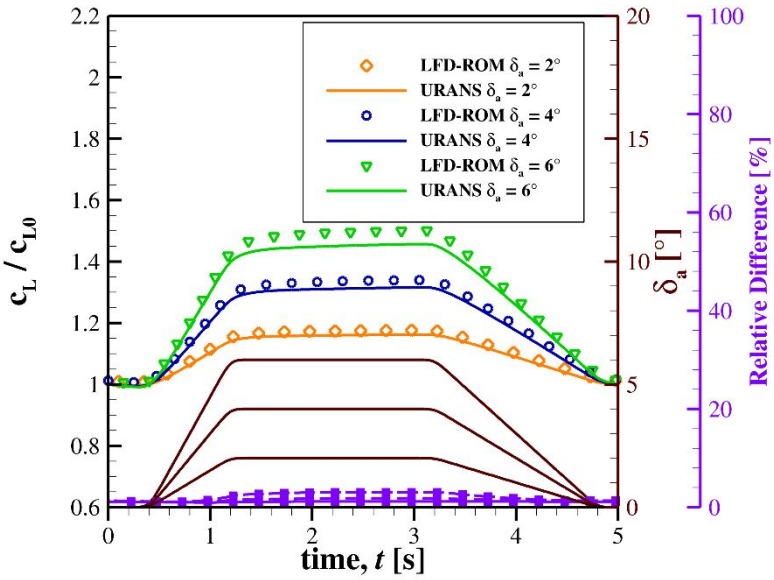

Figure 16. Aileron ROM's prediction vs URANS simulation results; trapezoid deflection profile. Flight condition: *Ma* = 0.24; *Re* = 2.1e7; *AoA* = 4°; *COR* = 0.73.

In the case of the aileron surrogate, deflections angles of 2°, 4°, and 6° were tested against their unsteady RANS counterpart to test for prediction validity. The results in Figure 16 above shows an average relative error between the two method of 0.4%, 0.6% and 1.1% for each angle respectively. This in general implies that: 1) the relative error remains rather small (around 1% or less) for angles up to 6° deflection and 2) the relative error is seen to increase with the deflection angle. However, 6° is already 60% of the overall deflection angle parameter range for which the surrogate was designed. Hence, 1.1%, can be seen as a very good estimation error in comparison to unsteady time-marching techniques, which would otherwise take longer to compute.

A further example in Figure 17 portrays a more arbitrary deflection profile: It approximates a zig-zag pattern of deflection, whereby from a stationary position, the aileron is simulated to deflect downwards up to a maximum angle of 9°, followed by a sudden return to an angle of 3°, and a subsequent deflection to an angle of 6°, before returning to the stationary position of 0°. Here, an improvement to the deflection pattern is made, whereby, a waiting period of around 4 sec is added prior to and after the deflection profile. The reason for this addition is the following: the LFD Method only computes periodic oscillations. As of such, the surrogate will include the influence of this periodicity in its predictions. Naturally, the aerodynamic response of a flow field responding to a control surface device deflecting from a stationary position is different from the response observable in a flow field already in tuned to a constant periodic oscillation. Also, the shorter the period of oscillation, i.e., the deflection profile's period, the more agitated the flow field, and as a consequence, the larger the expected disparity between the surrogate's prediction and the standard URANS technique. To minimize this

difference, the deflection profile is redefined. While the deflections of interest are at the centre of the complete deflection profile, a waiting period is added on either end, in order remove any extra harmonics which would model a continuous oscillation from the end of the deflection profile to the subsequent restart of it at the beginning. A flattened curve would indicate that the modes should cease at the end of the profile, to restart the deflection anew at T = 0 sec. Hence, the surrogate still predicts a periodic oscillation, but as a better approximate to the desired real scenario. The curves are also smoothened to replicated actuator systems better, since sharp turns can generate extreme accelerations which not only cause jerks, but also do not reflect realism in aileron movement. The following are the results of this test:

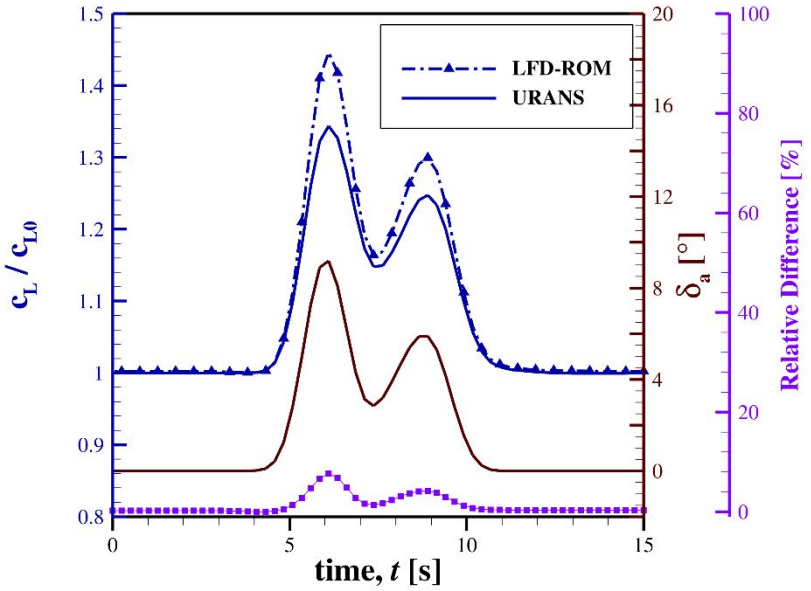

Figure 17. Aileron ROM's prediction vs URANS simulation results; zig-zag deflection. Flight condition: *Ma* = 0.21; *Re* = 1.8e7; *AoA* = 6.3°; *COR* = 0.81.

The relative difference recorded in Figure 17 is well under 10%. As the ROM's parameter space is indeed up to 10°, it is observed that an aileron deflection up to 9° still deliver a good prediction.

A point to note from Figure 16 and 17 above: the aileron surrogate consistently overpredicted the increase in lift coefficient as opposed to the URANS simulations. During an aileron deflection, any possible non-linearities could reduce the potential increase in lift coefficient. While this is captured by the URANS simulation study, the surrogate is incapable of doing so, as it is based upon a linear consideration.

The subsequent Figure 18 on the other hand describes the lift coefficient profile prediction of the spoiler surrogate model in comparison to instationary RANS simulations for angles 2°, 3°, and 4°. The spoiler ROM posed a greater challenge in modelling since only a linear flow field is valid for LFD predictions; hence the range of angles usable for the study and tests was fairly limited. Also, since within this range, non-linearity could still be a factor, albeit small, a greater disparity was observed between the test cases and their corresponding URANS computations. The tests concluded that the relative errors for the spoiler case were within 2.2% of their URANS counterpart. Despite being comparatively larger than the aileron case study, the errors recorded are still very small, and thus tolerable for the surrogate's potential use as a tool for load prediction and dynamic response analyses.

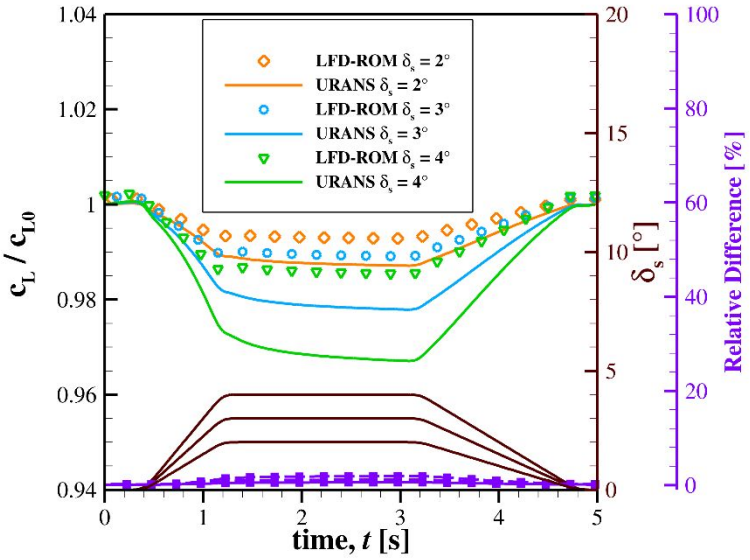

Figure 18. Spoiler ROM's prediction vs URANS simulation results; trapezoid deflection profile. Flight condition: *Ma* = 0.18; *Re* = 2.2e7; *AoA* = 3°; *COR* = 0.88.

Analogous to the aileron case, a zig-zag spoiler deflection was further simulated to compliment the above trapezoidal deflection profile study to validate the spoiler surrogate's prediction capability: this is portrayed in Figure 19 below. The same method of extending the overall deflection period was applied to this test case to model a real spoiler deflection better. An accuracy of less than 1.7% is observed compared to the unsteady simulation for the given flight condition (*Ma* = 0.25; *Re* = 3.2e7; *AoA* = 2.2°; *COR* = 0.87).

Once again, the disparity between the surrogate and the URANS method is due to non-linearities occurring during the deflection of the spoiler. The URANS technique captures these, while the surrogate cannot. Since the spoiler acts to break the flow and reduce lift, these added non-linearities cause further flow separation, worsening lift; hence, the drop in lift coefficient is larger in the URANS case, than predicted by the surrogate.

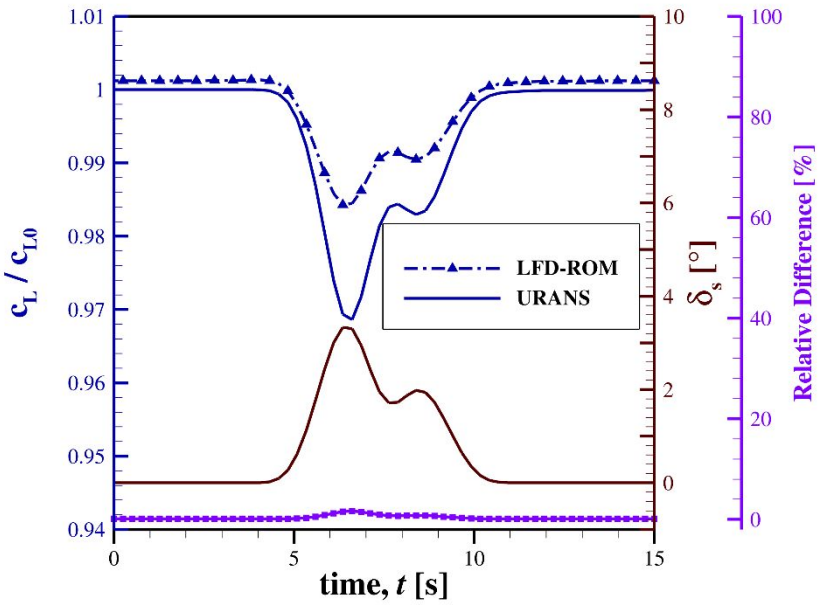

Figure 19. Spoiler ROM's prediction vs URANS simulation results; zig-zag deflection. Flight condition: *Ma* = 0.25; *Re* = 3.2e7; *AoA* = 2.2°; *COR* = 0.87.

Table III. URANS vs ROM Computation Time

URANS computation time / computed deflection angle point	6 sec
ROM computational time / flight condition	0.86 sec

Finally, a comparison is made between the URANS computation time with that of the surrogates in Table III. Since the URANS computation time was observed to increase, irrespective of flight conditions, proportionally to the number of deflection points computed, only the computation time per deflection angle point is listed. On the other hand, the ROM consistently clocked a computation time of around 1 sec or less, for all flight conditions tested. In general, the average computation time of the surrogate was 0.86 sec.

To compare the two computation periods, the following reasoning is applied. The proportionality factor for the URANS computation case, in relation to the number of deflection angle points computed, is 6 sec. On the other hand, the ROM's average computation is constant at 0.86 sec, irrespective of the number of deflection points computed. The ratio then, between the URANS computation and the ROM's computation time is in turn also proportional to the number of deflection points computed, with a proportionality factor of 7. Hence, it can be concluded, that the ROM's computation time advantage over the URANS technique increases 7-fold with an increasing number of deflection points computed.

13. CONCLUSION

To conclude, the surrogates showed a robustness in predicting dynamic responses for the given parameter combinations. The interpolation algorithm of the SMARTy toolbox provided sufficiently accurate results so long as the flight conditions remained close to the centre of the defined parameter space: only parameter combinations at the edge of the surrogate's parameter domain yielded large errors.

In general, the LFD procedure is an efficient means for dynamic response modelling, as the solutions are built upon RANS solutions, which aren't computationally expensive as opposed to unsteady time-marching simulations. The LFD solver of the DLR-TAU code computes rather economically, with 200 reduced frequencies computed in 45 minutes up to 1 hour with 1 node of the DLR CARA Cluster. This, including the RANS computation, would mean that the average computation time to produce a surrogate model, incorporating the full range of the defined parameter space, with the LFD technique, would be around 1 hour and 10 minutes. Considering the great number of possible parameter combinations, each researchable within 1 sec with the produced surrogate, this promises a massive time saving as opposed to the standard URANS method; the time it takes to compute just 1 flight condition with URANS is comparable to the time it takes to prepare the surrogate model depending on the number of deflection points computed.

The quality of the ROMs can be summed up as follows: The Leave-One-Out tests produced results of under 15% for the aileron case and 13.5% for the spoiler case. These were, however, the most extreme outliers for

each case, with much of the cases being accurate well under 10% across the ROM's parameter domain. The surrogates are thus reliable for predicting results, even for the more challenging case of the spoiler surrogate.

A special mention must be made here in regards to surrogate modeling spoilers with LFD. Since spoilers function specifically to break the flow to reduce lift while increasing drag, it was exceptionally difficult to find the "sweet" zone where the flow field still remained stable and thus linear enough for valid RANS-LFD solutions to be produced. Hence the range of usable deflection angles for this device was rather restricted to within 5°. Naturally the fully deflected fowler flap present in the high-lift-device configuration in this study contributed greatly to the flow field being rather unsteady beyond 5° of spoiler deflection angle.

Lastly, the applicability of both surrogates was proven in Section 12. Precise predictions were seen as possible by the surrogate, reflecting their URANS counterpart with a difference of within 10% for the defined parameter domain. The RANS-LFD surrogates portrayed a liability towards non-linear flow effects which may occur during a real control surface deflection: this caused the aileron surrogate to overpredict increases in lift, while the spoiler surrogate underpredicted the drop in lift coefficient, in comparison to the URANS simulation studies conducted. The engineer should note this characteristic when using such ROMs. Time saving was also proven true with the surrogate, as the computation time advantage of the ROM increases, by a factor of 7, as the deflection profile's resolution increases. Hence it would be in fact preferable, to make the desired deflection profile as well defined as possible, as this would mean a more worth-while use of the surrogate, while also enabling a more precise result to be produced by the ROM.

14. LIMITATION & RECOMMENDATIONS

Linearity if of utmost importance for LFD. The LFD method is therefore best suited to those flight regimes which best promote linearity.

Generally, in regards to both devices, should the parameter space need to be enlarged, the snapshots must be similar in nature and abrupt flow changes should be avoided within the surrogate as it would reduce interpolation accuracy. Alternatively, multiple surrogates can be prepared across a wide parameter space.

REFERENCES

Berblinger, M. and Schlier, C. (1991), "Monte Carlo integration with quasi-random numbers: some experience", *Computer Physics Communications*, Vol. 66 (2-3), pp. 157-166, doi: 10.1016/0010-4655(91)90064-R. ISSN 0010-4655.

Berkooz, G., Holmes, P. and Lumley, J. L. (1993), "The Proper Orthogonal Decomposition in the analysis of turbulent flows", *Annual Review of Fluid Mechanics*, Vol. 25, pp. 539-575, doi:10.1146/annurev.fl.25.010193.002543.

Dolci, V. and Arina, R. (2016), "Proper Orthogonal Decomposition as surrogate model for aerodynamic optimization", *International Journal of Aerospace Engineering*, Vol. 2016, Article ID 8092924, doi: 10.1155/2016/8092824.

Halton, J. H. (1960), "On the efficiency of certain quasi-random sequences of points in evaluating multi-dimensional integrals", *Numerische Mathematik*, Vol. 2, pp.84-90.

Ripepi, M., Verveld, M. J., Karcher, N. W., Franz, T. and *et al.* (2018), "Reduced Order Models for aerodynamic applications, load and MDO", *CEAS Aeronautical Journal*, Vol. 9, pp. 171-193, doi: 10.1007/s13272-018-0283-6.

Seidler, R.B., Marten, S., Widhalm, M. and Wild, J. (2019), "Efficient prediction of aerodynamic response behavior for control surfaces using the Linear Frequency Domain", *AIAA Journal*, Vol. 58, No. 5, doi: 10.2514/1.J058840.

Spalart, P. and Allmaras. S. (1992), "A one-equation turbulence model for aerodynamic flows", *30th Aerospace Sciences Meeting and Exhibit*, doi: 10.2514/6.1992-439.

Widhalm, M., and Thormann, R. (2017), "Efficient evaluation of dynamic response data with a linearized frequency domain solver at transonic separated flow conditions", *AIAA Paper*, pp. 1-6, doi: 10.2514/6.2017-3905.

FIGURES

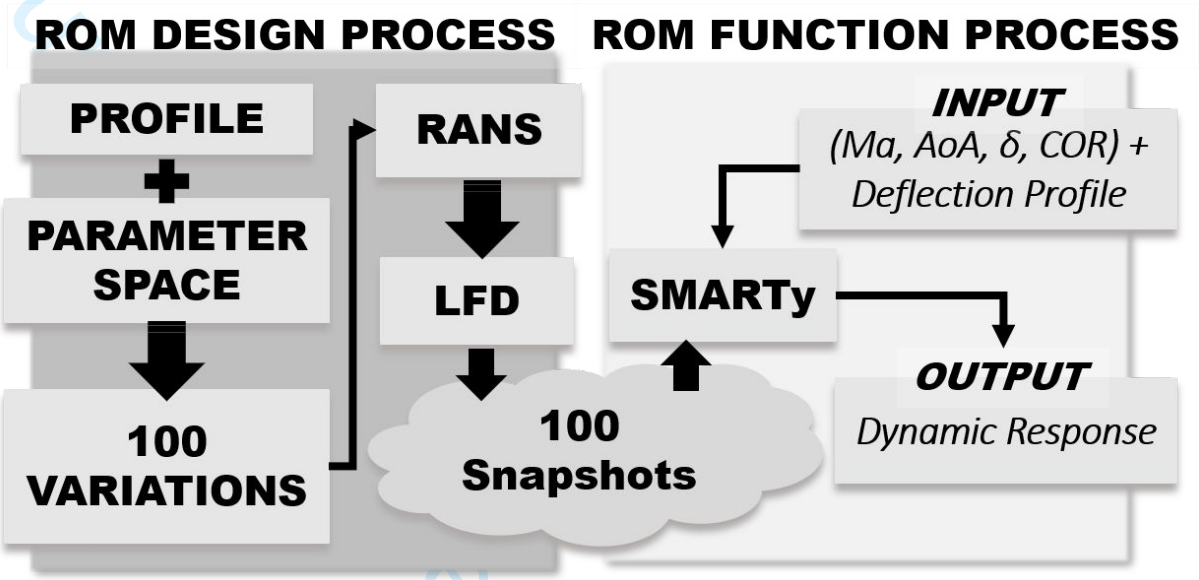

Figure 1. Surrogate design and function process chain.

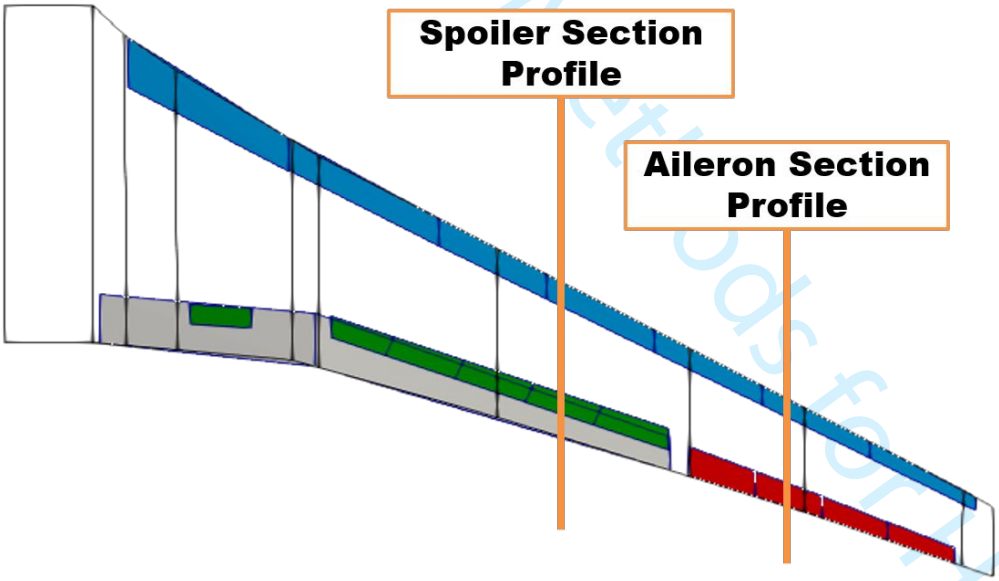

Figure 2. Control surface layout of the XRF1 Concept Aircraft.

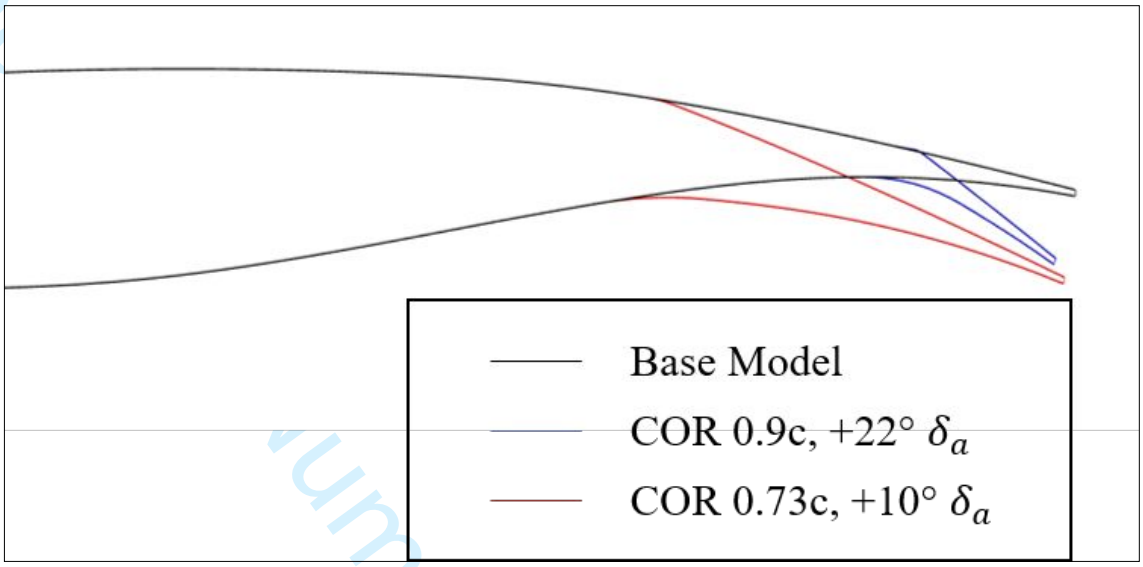

Figure 3. Modelling of the aileron deflection.

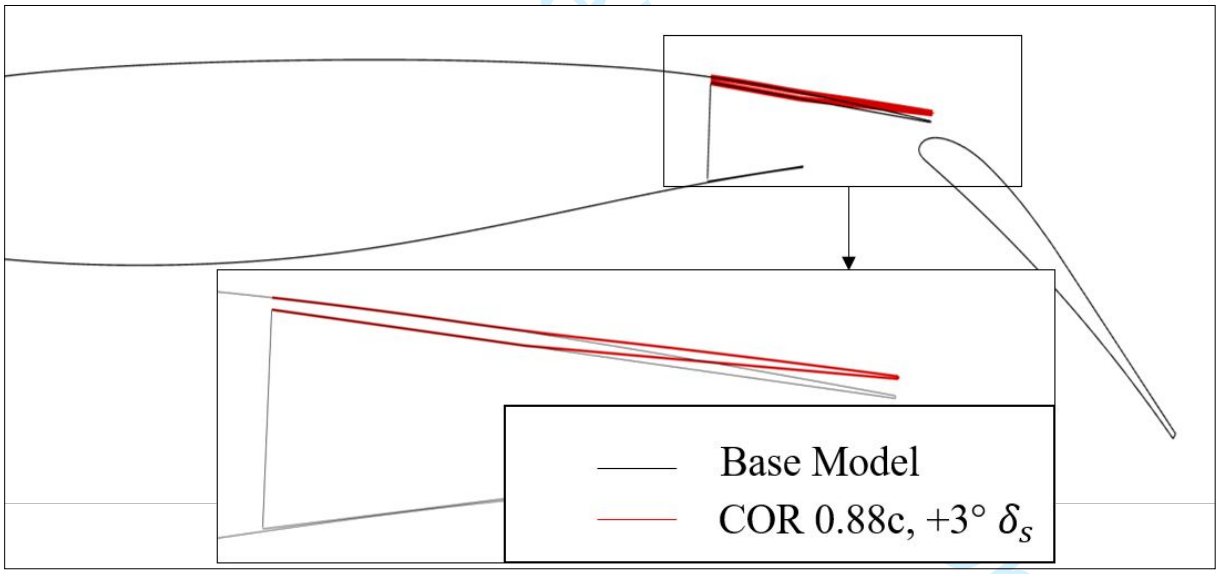

Figure 4. Modelling of the spoiler deflection.

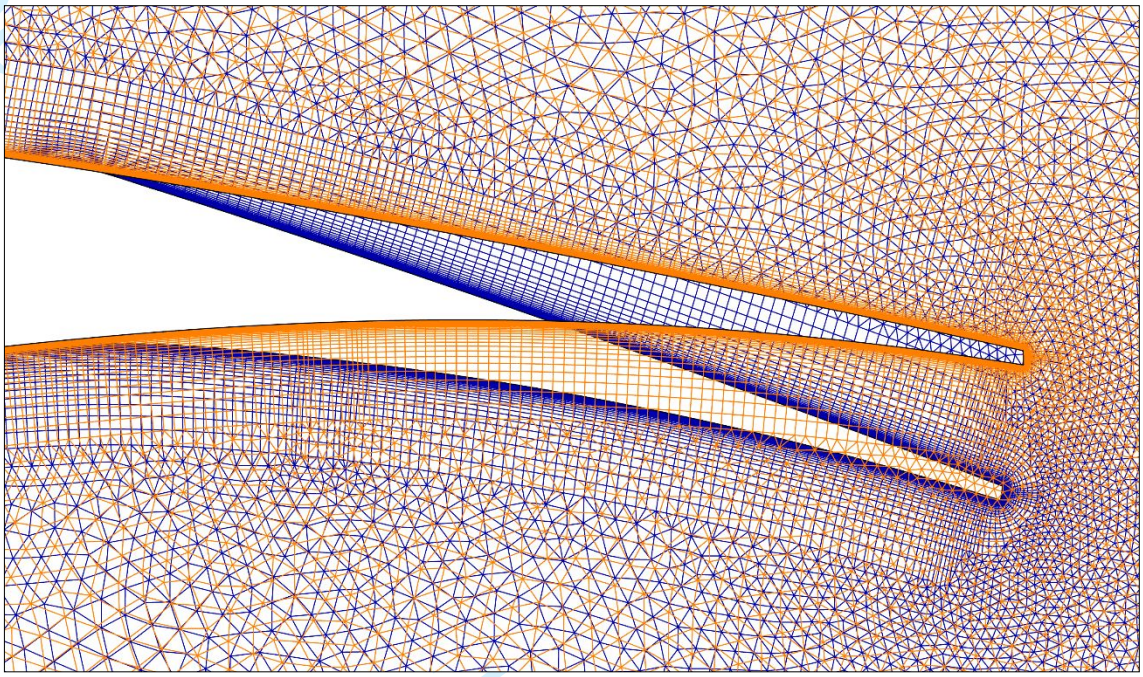

Figure 5. Mesh deformation of the aileron section (COR at 76% chord length; deflection angle: 8.52°).

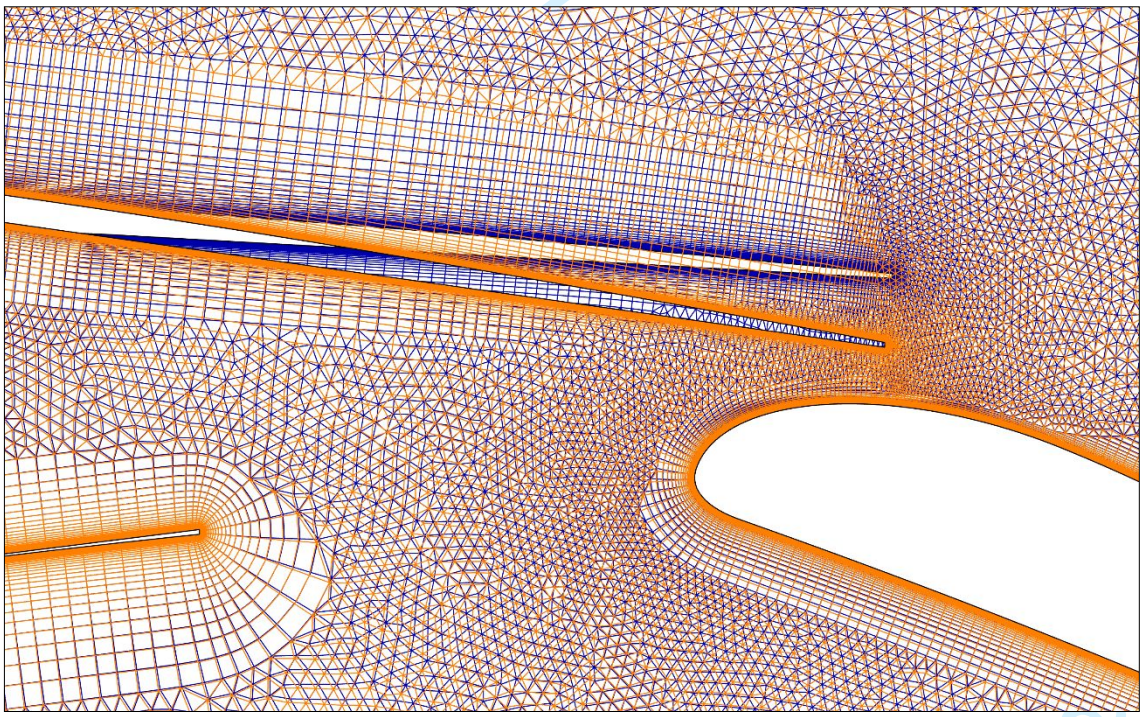

Figure 6. Mesh deformation of the spoiler section (*COR* at 86% chord length; deflection angle: 4.51°).

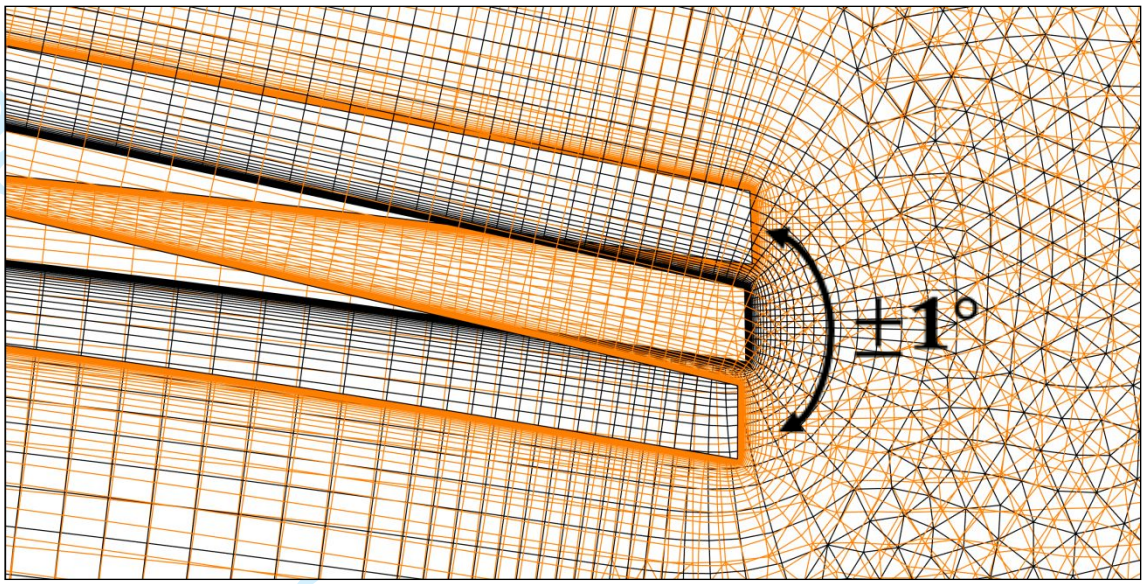

Figure 7. Modelling of a ±1-degree aileron deflection in DLR-TAU Code with the Radial Basis Function Method.

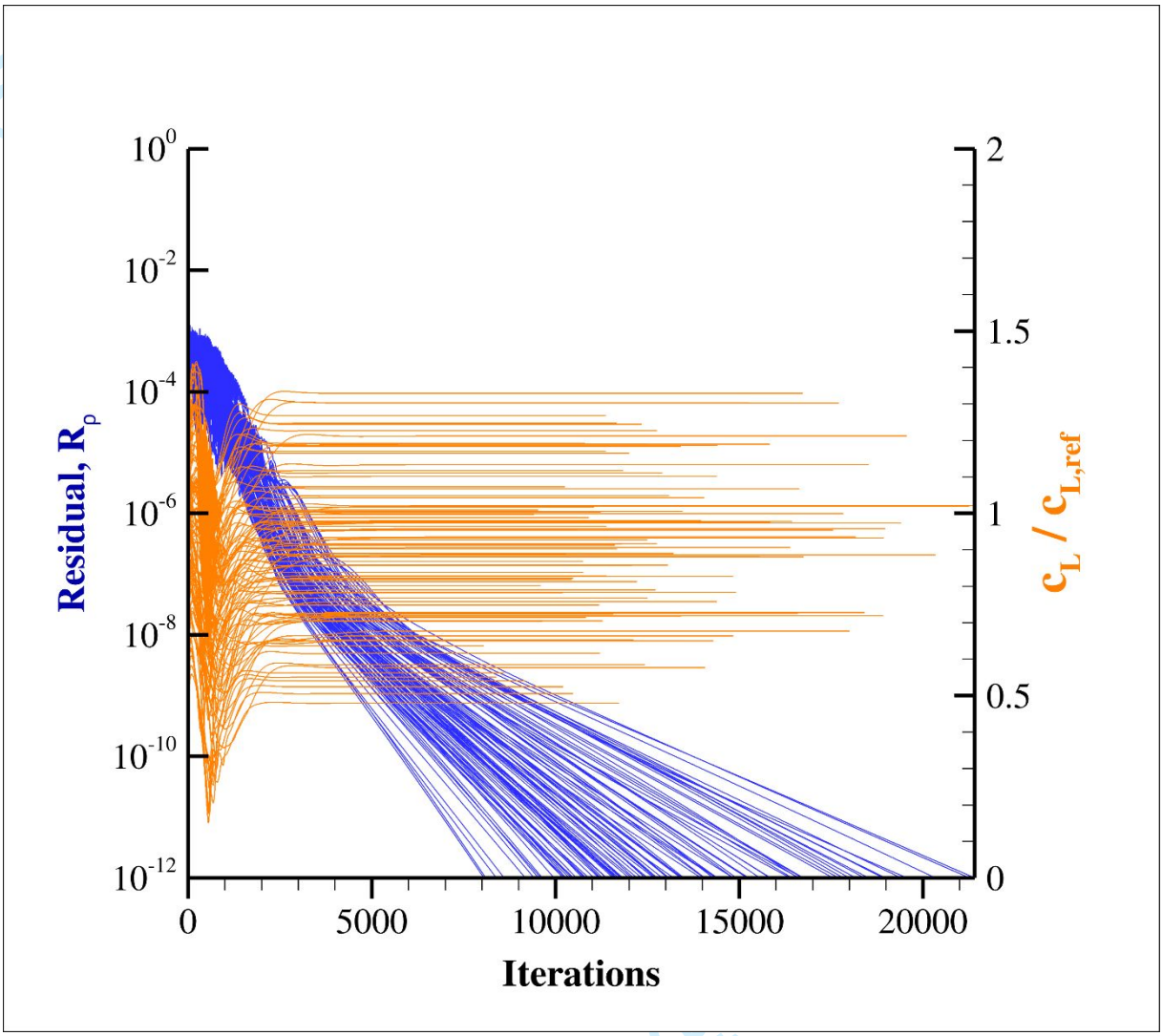

Figure 8. RANS solution for Halton sequence of 100 parameter combinations (Aileron section profile in take-off configuration with 15° slat and 10° flap deflection at mean sea level (MSL) conditions); Reference flight condition: Ma = 0.25; Re = 2.2e7; AoA = 7.02°; δ_a = 3.28°; COR = 0.9.

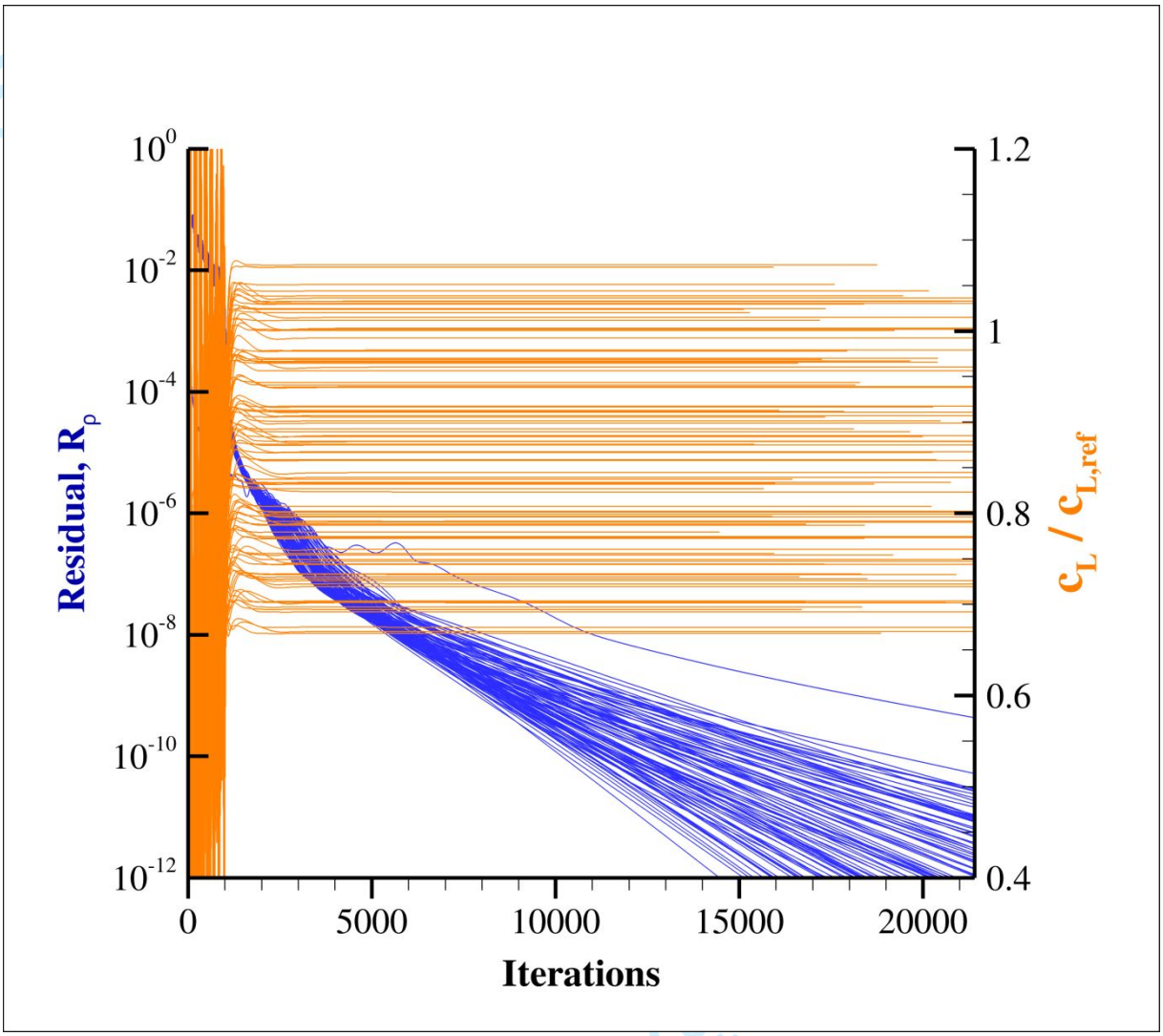

Figure 9. RANS solution for Halton sequence of 100 parameter combination (Spoiler section profile in take-off configuration with 15° slat and 10° flap deflection at mean sea level (MSL) condition); Reference flight condition: Ma = 0.25; Re = 3.2e7; AoA = 7.02°; δ_s = 3.36°; COR = 0.9.

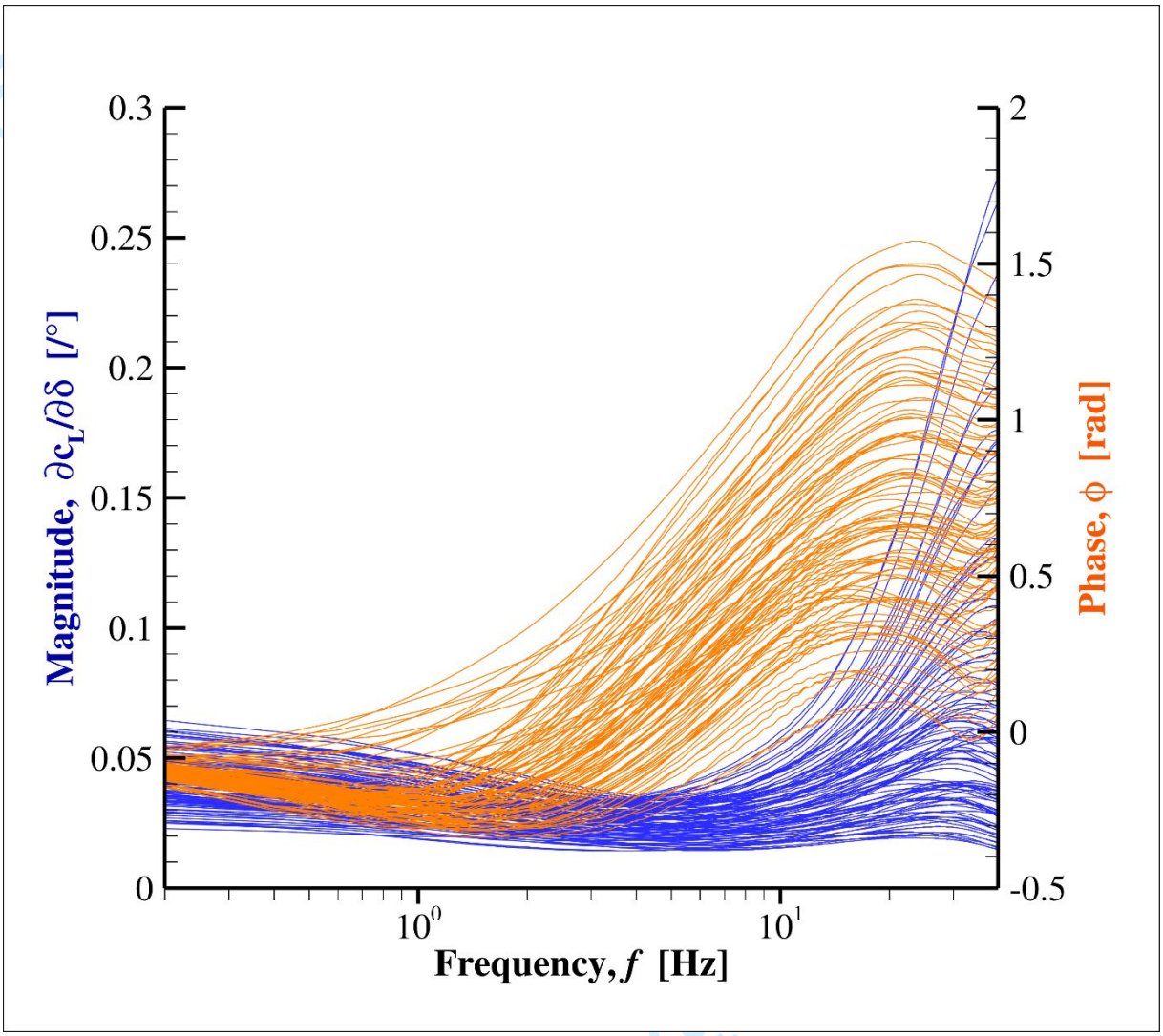

Figure 10. Magnitude and phase diagram of the dynamic responses for an aileron deflection over a frequency range of 0 - 40 Hz.

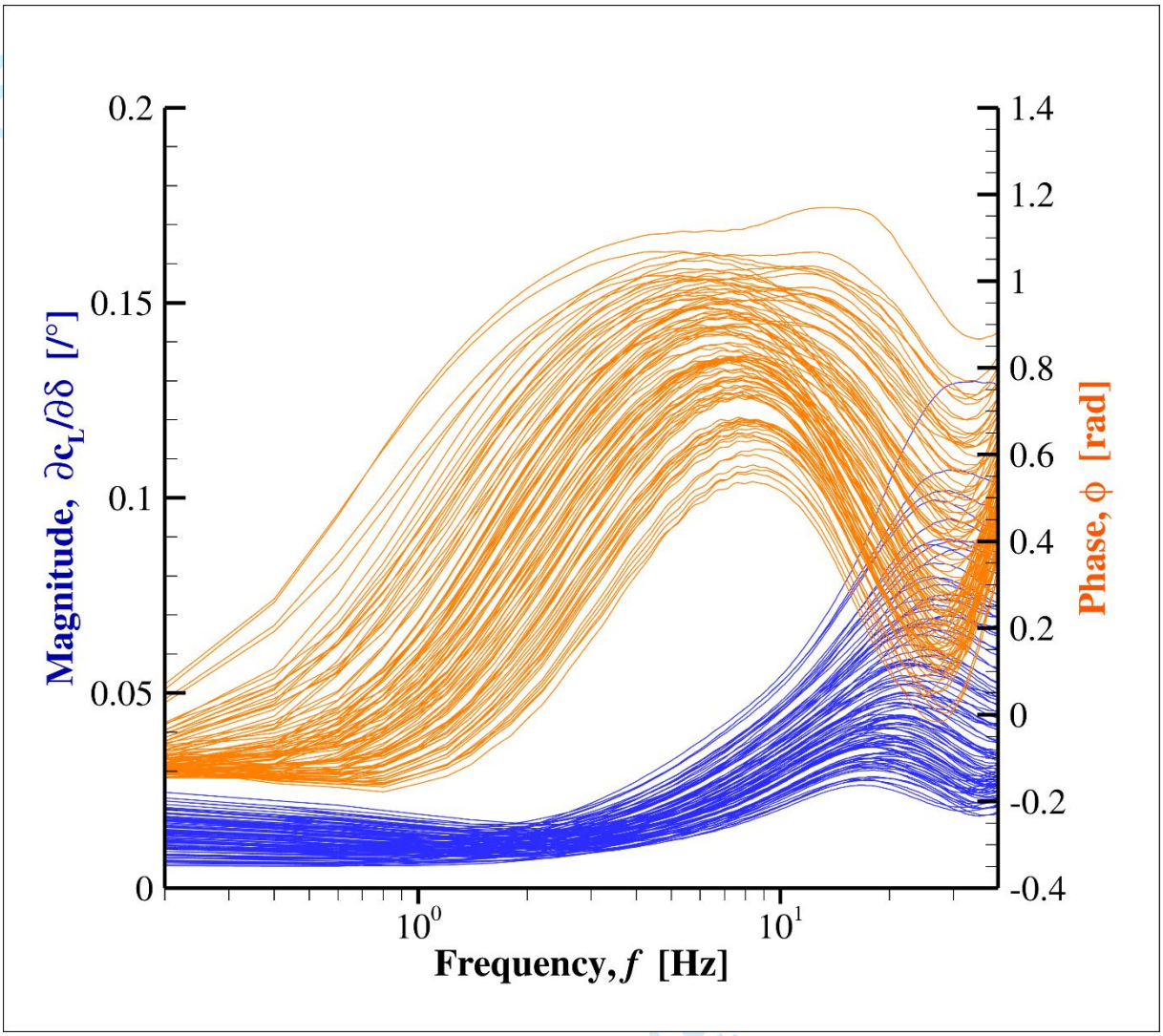

Figure 11. Magnitude and phase diagram of the dynamic responses for a spoiler deflection over a frequency range of 0 - 40 Hz.

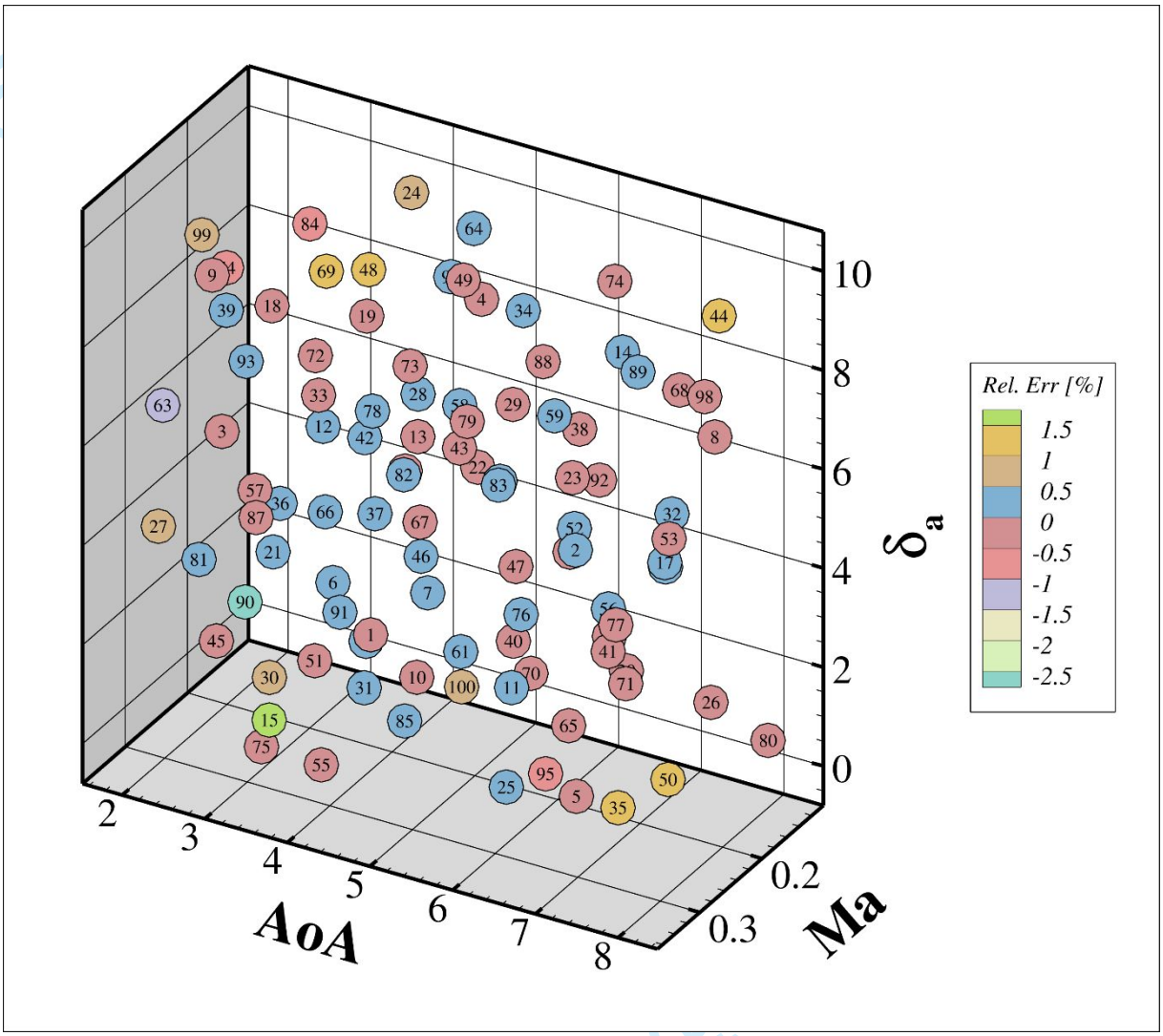

Figure 12. 3D plot of the aileron surrogate's Leave-One-Out Test for the interpolation of the static section lift coefficient, c_L; data points numbered according to Halton sequence.

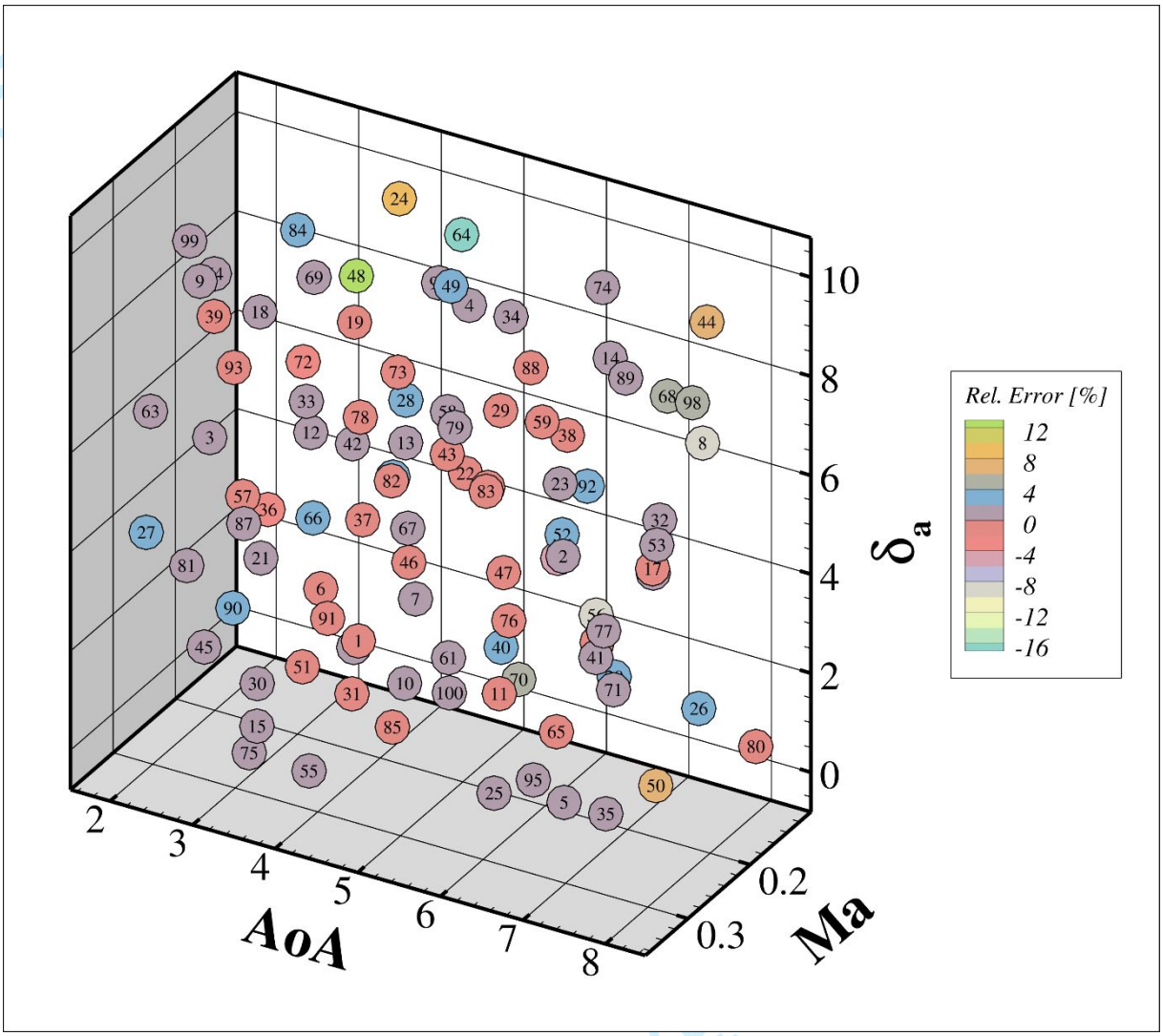

Figure 13. 3D plot of the aileron surrogate's Leave-One-Out Test for the interpolation of the dynamic response; data points numbered according to Halton sequence.

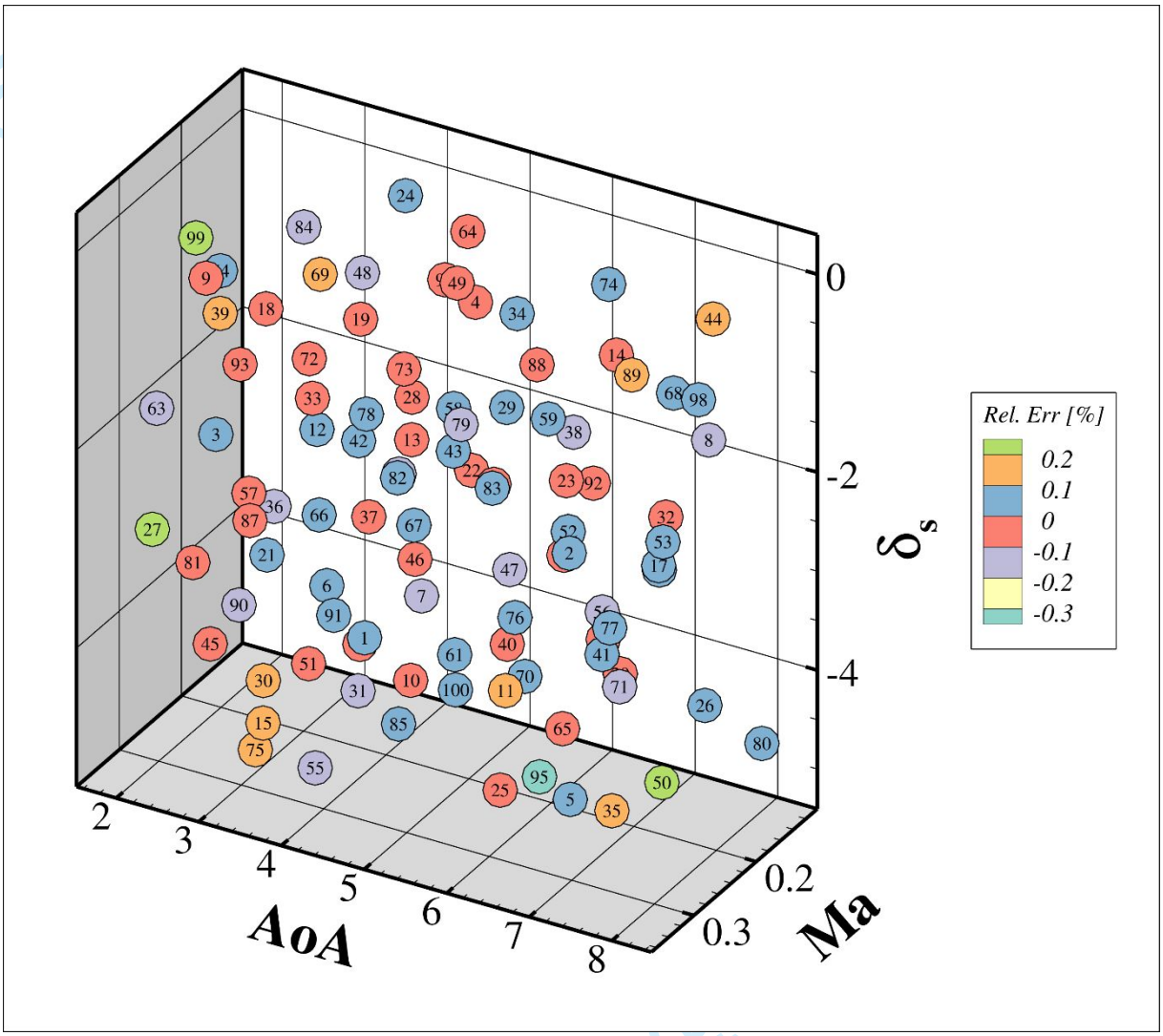

Figure 14. 3D plot of the spoiler surrogate's Leave-One-Out Test for the interpolation of the static section lift coefficient, c_L; data points numbered according to Halton sequence.

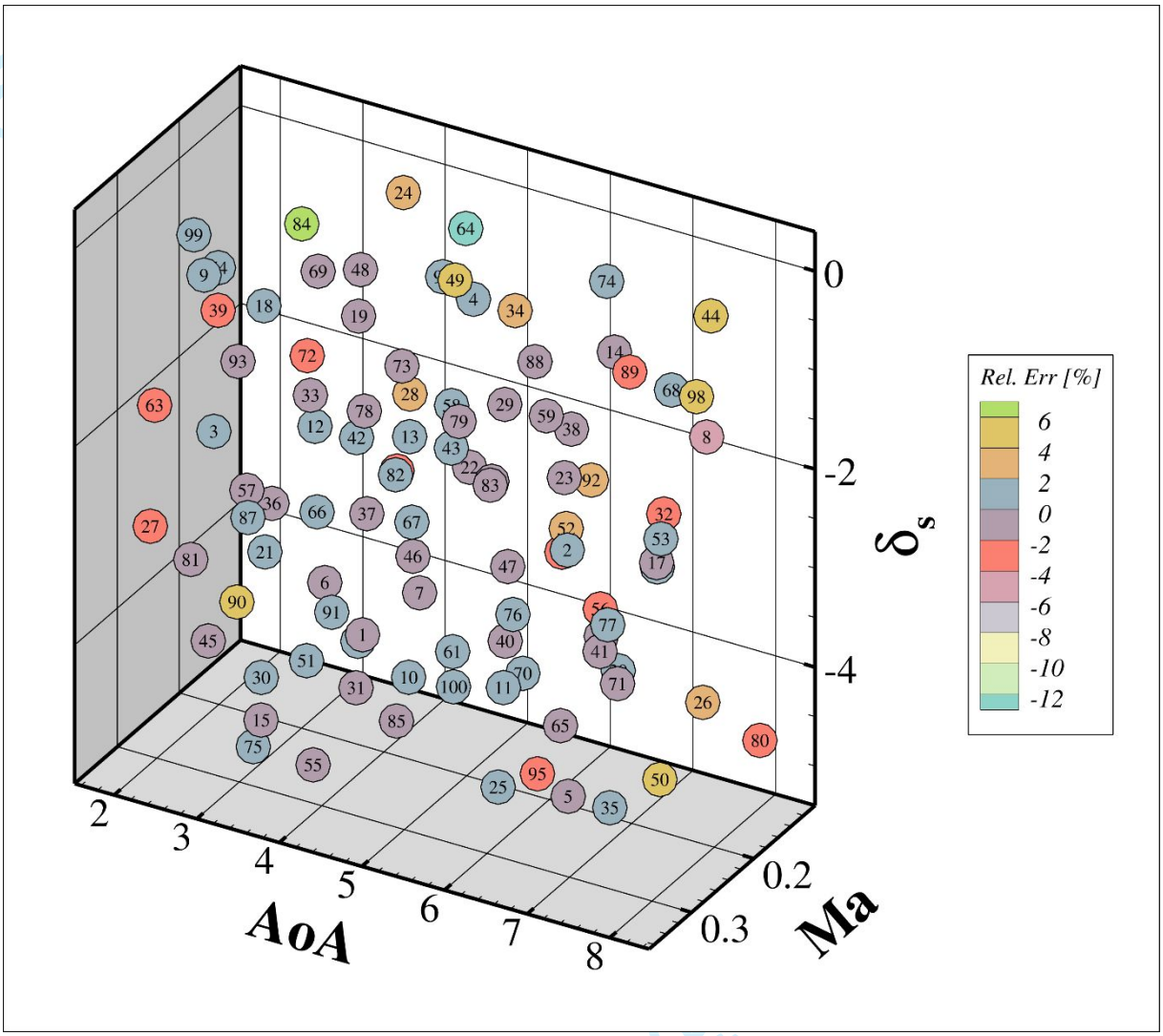

Figure 15. 3D plot of the spoiler surrogate's Leave-One-Out Test for the interpolation of the dynamic response; data points numbered according to Halton sequence.

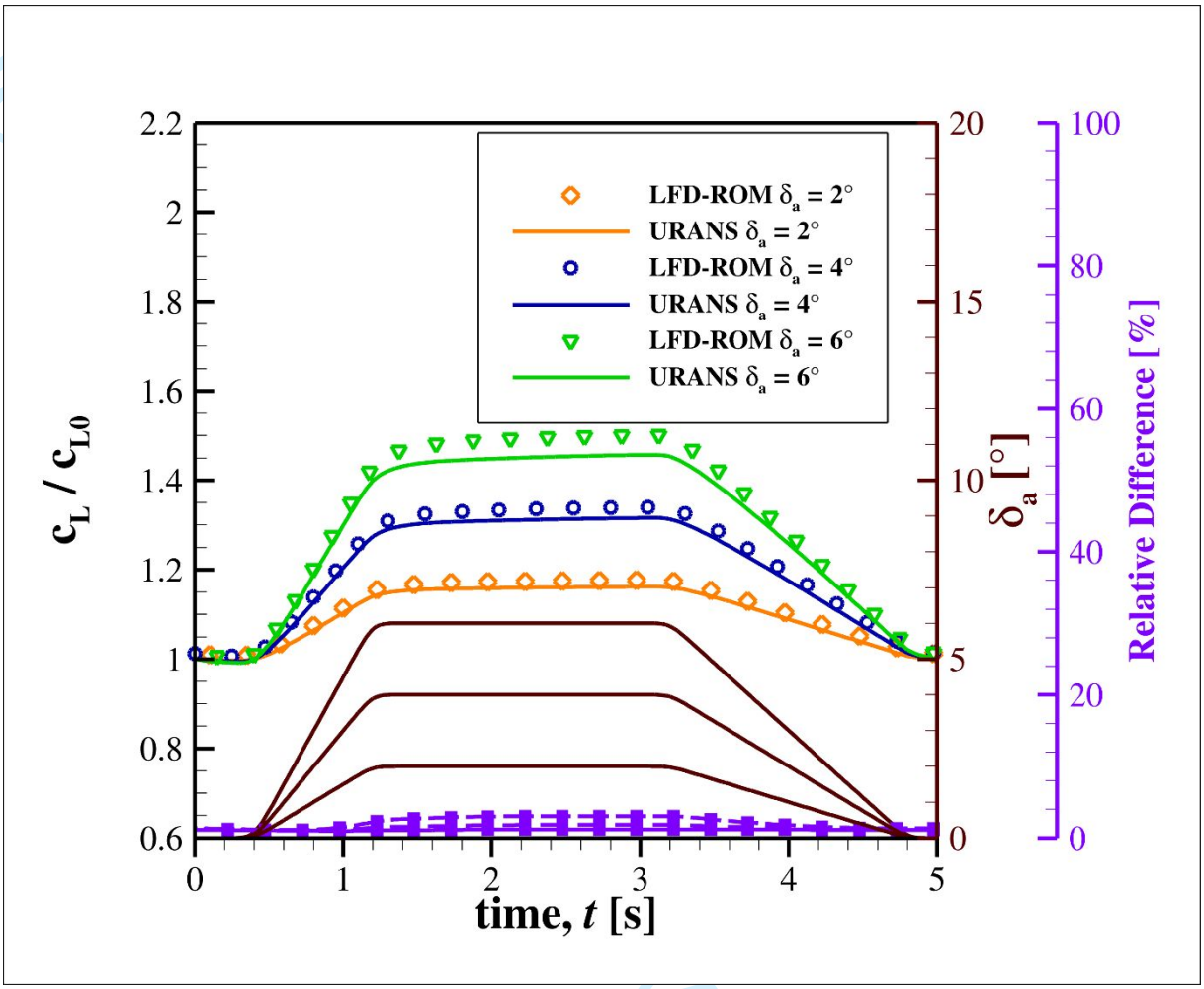

Figure 16. Aileron ROM's prediction vs URANS simulation results; trapezoid deflection profile. Flight condition: *Ma* = 0.24; *Re* = 2.1e7; *AoA* = 4°; *COR* = 0.73.

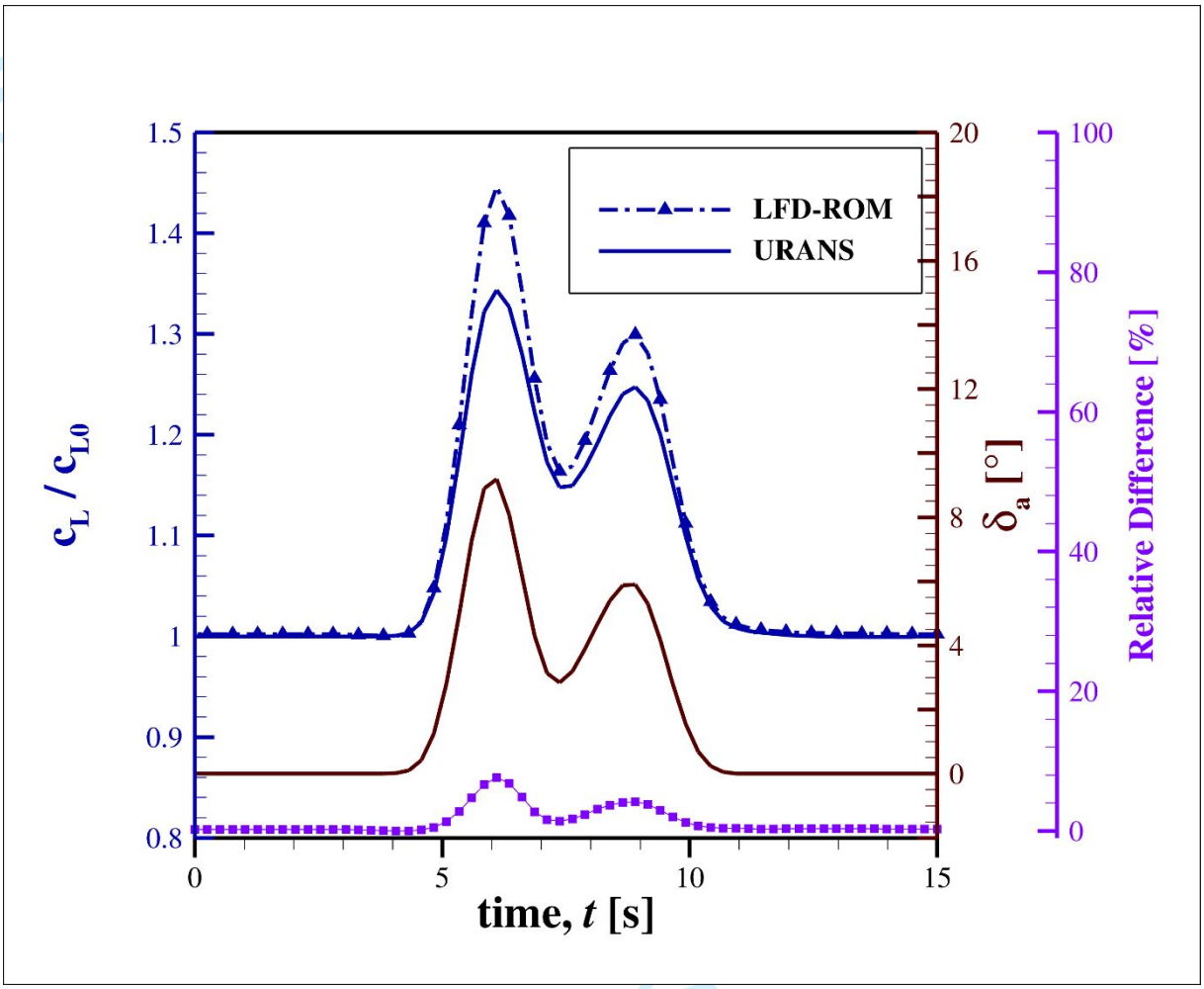

Figure 17. Aileron ROM's prediction vs URANS simulation results; zig-zag deflection. Flight condition: *Ma* = 0.21; *Re* = 1.8e7; *AoA* = 6.3°; *COR* = 0.81.

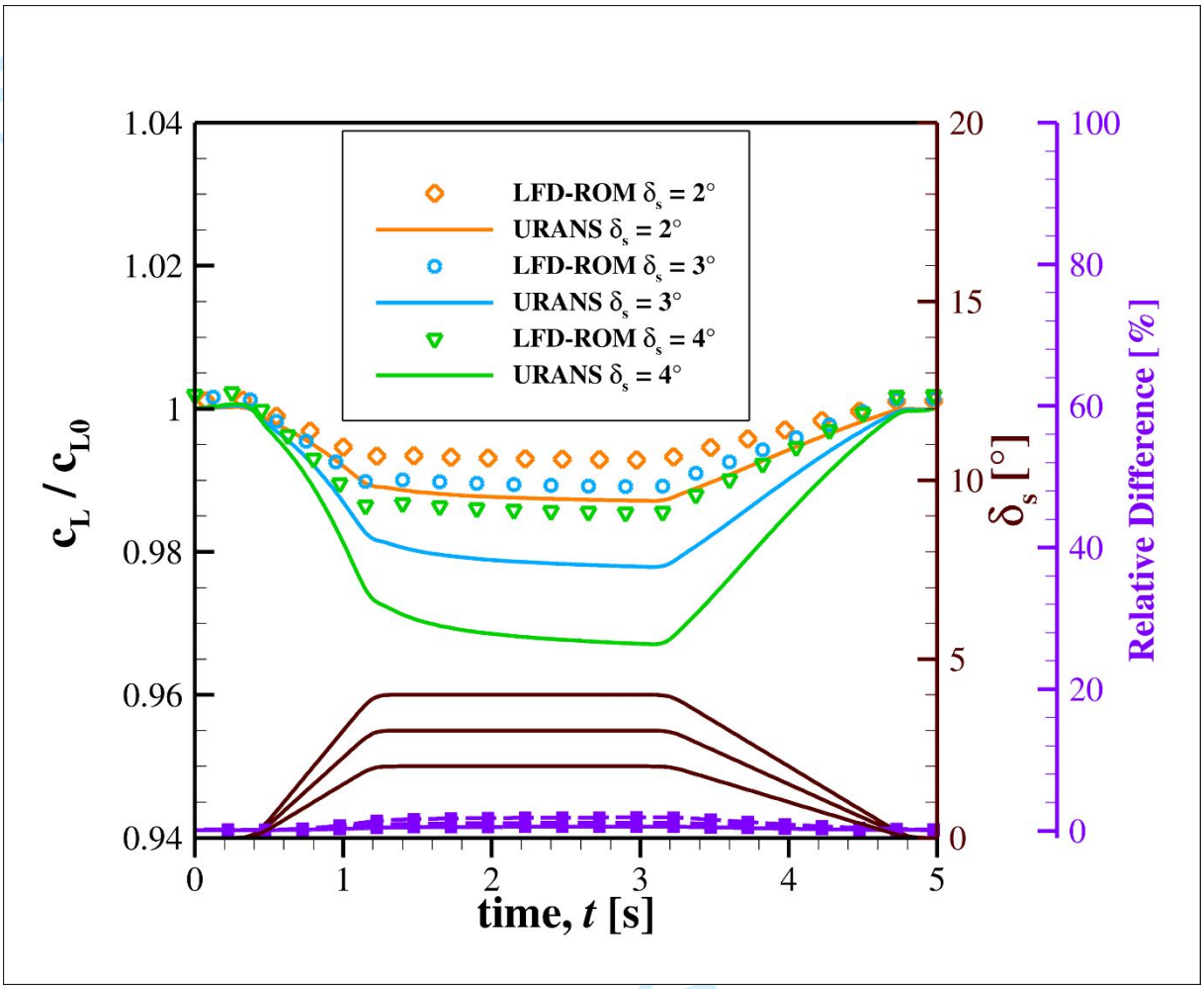

Figure 18. Spoiler ROM's prediction vs URANS simulation results; trapezoid deflection profile. Flight condition: *Ma* = 0.18; *Re* = 2.2e7; *AoA* = 3°; *COR* = 0.88.

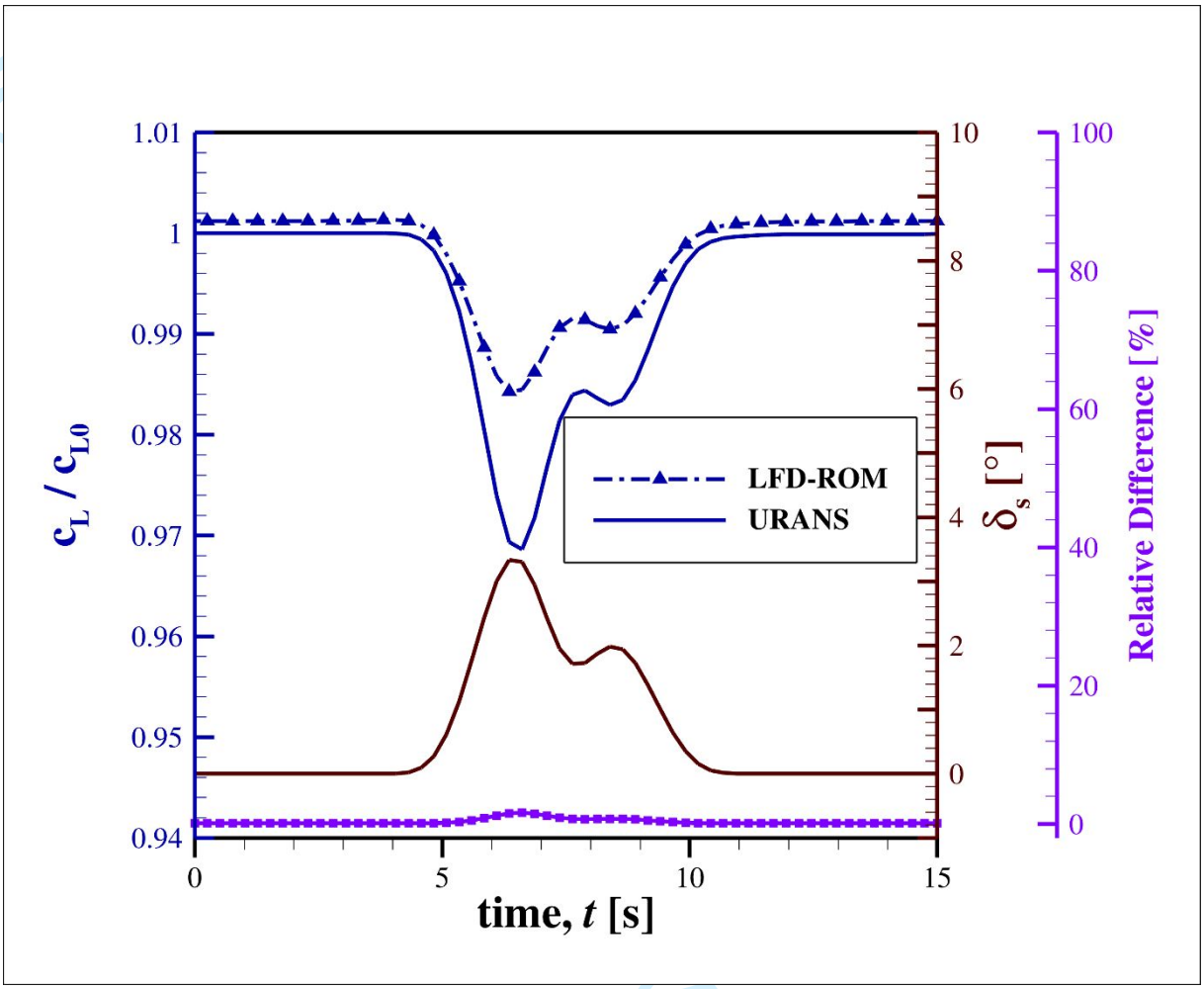

Figure 19. Spoiler ROM's prediction vs URANS simulation results; zig-zag deflection. Flight condition: *Ma* = 0.25; *Re* = 3.2e7; *AoA* = 2.2°; *COR* = 0.87.

TABLES

Table I. Aileron Surrogate's Parameter Space

Mach number, *Ma*	0.12 - 0.35
Reynolds number, *Re*	1.2e7- 3e7
Angle of attack, *AoA*	2° - 8°
Aileron deflection angle, δ_a	0 - +10°
Ratio of aileron chord to profile chord	0.1 – 0.3

Table II. Spoiler Surrogate's Parameter Space

Mach number, Ma	0.12 - 0.35
Reynolds number, Re	1.2e7 - 3e7
Angle of attack, AoA	2° - 8°
Spoiler deflection angle, δ_s	0 - +5°
Ratio of spoiler chord to profile chord	0.1 - 0.15

Table III. URANS vs ROM Computation Time

URANS computation time / computed deflection angle point	6 sec
ROM computational time / flight condition	0.86 sec